PLOS Pathogens

RESEARCH ARTICLE

Evaluating beta-tubulin variants as predictors of benzimidazole resistance across *Caenorhabditis* nematodes

Amanda O. Shaver[1☯], Ryan McKeown[2☯], Joyce M. Reyes Otero[3], J.B. Collins[1], Daniel W. Hogan[4], James S. Fraser[4], Stephen M. Dreyer[5], Erik J. Ragsdale[5], Erik C. Andersen[1*]

1 Department of Biology, Johns Hopkins University, Baltimore, Maryland, United States of America, **2** Department of Molecular Biosciences, Northwestern University, Evanston, Illinois, United States of America, **3** Department of Biology, University of Puerto Rico, San Juan, Puerto Rico, **4** Department of Bioengineering and Therapeutic Sciences, University of California San Francisco, San Francisco, California, United States of America, **5** Department of Biology, Indiana University, Bloomington, Indiana, United States of America

☯ These authors contributed equally to this work.
* erik.andersen@gmail.com

Citation: Shaver AO, McKeown R, Reyes Otero JM, Collins JB, Hogan DW, Fraser JS, et al. (2026) Evaluating beta-tubulin variants as predictors of benzimidazole resistance across *Caenorhabditis* nematodes. PLoS Pathog 22(6): e1014306. https://doi.org/10.1371/journal.ppat.1014306

Editor: Krishanpal Karmodiya, Indian Institute of Science Education and Research, Pune, INDIA

Received: January 20, 2026

Accepted: May 27, 2026

Published: June 5, 2026

Data availability statement: All code and data used to replicate the data analysis and figures are available on GitHub at: https://github.com/AndersenLab/ce_cb_ct_betatubulin. S1 Table contains the list of C. elegans isotype reference strains, any beta-tubulin variants, sample collection locations, and substrate types. S2

Abstract

Benzimidazoles, a widely used class of anthelmintic drugs, target beta-tubulin, disrupt microtubule formation, and delay nematode development. In parasitic nematodes, mutations in beta-tubulin genes are predicted to inhibit benzimidazole binding and are associated with resistance. In the free-living nematode *Caenorhabditis elegans*, loss-of-function mutations in the beta-tubulin gene *ben-1* cause benzimidazole resistance. Although several beta-tubulin mutations serve as established markers of resistance, the prediction of the effects of novel variants in different nematode species remains challenging. Here, we identified novel beta-tubulin variants predicted to confer benzimidazole resistance across wild strains in three *Caenorhabditis* species: *C. elegans*, *Caenorhabditis briggsae*, and *Caenorhabditis tropicalis*. The three *Caenorhabditis* species are experimentally tractable, have characterized beta-tubulin gene complements, and defined natural niches, which allowed us to identify variants in beta-tubulin genes and test which variants are associated with resistance. We hypothesized that, if these species experienced similar selective pressures, they would evolve resistance to benzimidazoles by mutations in a beta-tubulin gene (*tbb-1*, *tbb-2*, *mec-7*, *tbb-4*, and *ben-1*). In the three *Caenorhabditis* species, we tested all strains harboring variants in the five conserved beta-tubulin genes for benzimidazole resistance. In *C. elegans*, we found that a heterogeneous set of variants in *ben-1* were associated with resistance. By contrast, only two variants in *C. briggsae ben-1* (W21stop and Q134H) were associated with resistance, suggesting selection acts differently in *C. briggsae* than in *C. elegans* despite overlapping geographic ranges between the two species. *C. tropicalis* was distinct from the other two species, where no strains with variants in any beta-tubulin gene were resistant. We generated

Table contains the list of C. briggsae isotype reference strains, any beta-tubulin variants, sample collection locations, and substrate types. S3 Table contains the list of C. tropicalis isotype reference strains, any beta-tubulin variants, sample collection locations, and substrate types. S4 Table contains all C. briggsae and C. tropicalis isotype reference strains with beta-tubulin variants and genetically related strains. S5 Table contains details about the CRISPR-Cas9 genome-edited strains, CRISPR-Cas9 reagents, and oligonucleotide sequences for the deletion of ben-1 in C. briggsae and C. tropicalis. S6 Table contains the results from the fecundity assays of the C. briggsae reference strain (AF16) and the Cbr-ben-1 deletion strains. Table S7 contains the results from the fecundity assays of the C. tropicalis strain NIC58 and the Ctr-ben-1 deletion strains. S8 Table contains the BLOSUM62 and Granthum scores for amino acid changes in the beta-tubulin genes in the three Caenorhabditis species. S9 Table contains expression breadth (Tau) estimates for beta-tubulin genes calculated on C. elegans and C. briggsae embryonic cells by Large et al. 2024. S10 Table contains conservation estimates of embryonic expression patterns between C. elegans and C. briggsae with Jensen-Shannon gene distances estimated in Large et al. 2024 for beta-tubulin genes. S11 Table contains the neuronal cell-class expression divergence of beta-tubulin orthologs across C. elegans, C. briggsae, and C. tropicalis, reported as Jaccard distances obtained from Toker et al. 2025. S12 Table contains results from the substrate enrichment analysis. S13 Table contains details about the CRISPR-Cas9 genome edited strains, CRISPR-Cas9 reagents, and oligonucleotide sequences for the deletion of ben-1 in P. pacificus. S14 Table contains all beta-tubulin transcript IDs in the three Caenorhabditis species. S15 Table contains the manual curation of SVs found in beta-tubulin genes. S16 Table contains the amino acid sequences for the BEN-1 proteins from the three Caenorhabditis species.

Funding: A.O.S. was funded by the National Institutes of Health grant F32AI181342 (https://www.niaid.nih.gov/). This work was supported by the National Institutes of Health grant R01AI153088 to E.C.A (https://www.niaid.nih.gov/). The funders had no role in study design, data collection and analysis, decision to publish, or preparation of the manuscript.

Competing interests: The authors have declared that no competing interests exist.

deletions of *ben-1* in *C. briggsae* and *C. tropicalis* and confirmed that loss of *ben-1* confers resistance in both species. Our findings reveal species-specific patterns of beta-tubulin-mediated benzimidazole resistance and emphasize that prediction of variants in beta-tubulin genes alone is not sufficient to predict resistance, especially across diverse *Caenorhabditis* species.

Author summary

Mutations in beta-tubulin genes have been associated with benzimidazole resistance across nematode species, yet predicting novel resistance variants remains challenging. Using wild strains from three *Caenorhabditis* species, we identified strains with variants in beta-tubulin genes and tested each strain for benzimidazole resistance. In *C. elegans,* a diverse set of loss-of-function variants in *ben-1* were associated with resistance. Whereas in *C. briggsae*, only two *ben-1* alleles were associated with resistance, suggesting selection acts differently in this species despite a similar niche as *C. elegans*. *C. tropicalis* had no strains with beta-tubulin variants that were resistant. Our results highlight species-specific patterns of benzimidazole resistance.

Introduction

Global control of parasitic nematode infections relies on the efficacy of a small arsenal of anthelmintic drugs, including benzimidazoles (BZs) [1]. BZs are a widely used class of anthelmintic drugs that inhibit the polymerization of microtubules [2–4] and delay nematode development [5]. Although BZs are essential to human and veterinary health, resistance is prominent in parasitic nematode populations [6,7]. In clade V nematodes (*e.g.*, *Ancylostoma caninum*, *Ancylostoma duodenale*, *Caenorhabditis elegans*, *Haemonchus contortus*, *Necator americanus*, *Teladorsagia circumcincta*, and *Trichostrongylus colubriformis*), BZ resistance is associated with mutations in beta-tubulin genes [8–16].

Among parasitic nematodes, BZ resistance has been best characterized in the small ruminant parasite *H. contortus* [17]. The *H. contortus* genome contains four genes that encode beta-tubulins (*tbb-isotype-1*, *tbb-isotype-2*, *tbb-isotype-3*, and *tbb-isotype-4*), where each encoded protein has a phenylalanine at position 200, which is thought to confer binding to BZs [18]. In field populations of *H. contortus*, BZ resistance has been historically associated with three canonical missense variants (F167Y, E198A, and F200Y) in *tbb-isotype-1* [19–22]. Recently, additional novel missense variants in *tbb-isotype-1* have been associated with *H. contortus* BZ resistance (*e.g.*, E198I, E198K, E198T, and E198stop) [23]. Except for E198stop, these newly described missense variants in *tbb-isotype-1* are hypothesized to disrupt BZ binding, without causing loss-of-function (LoF). Given the high expression of *tbb-isotype-1* and the presence of change-of-function missense variants (rather than LoF variants)

in resistant populations, *tbb-isotype-1* is likely an essential beta-tubulin in *H. contortus* [18]. By contrast, *tbb-isotype-2* LoF alleles have been identified in highly resistant *H. contortus* populations [24], indicating that it is not an essential gene. However, *tbb-isotype-2* LoF alleles have only been observed alongside resistance-associated *tbb-isotype-1* alleles, making it unclear whether *tbb-isotype-2* LoF alleles can independently confer resistance in *H. contortus* populations [18]. The other two beta-tubulin genes are expressed at low levels and have not been associated with BZ resistance [18]. The beta-tubulin genes and alleles involved in BZ resistance suggest that specific variants that prevent or reduce BZ binding can be tolerated, whereas complete loss of essential beta-tubulin genes cannot.

Unlike *H. contortus*, the free-living model nematode species *C. elegans* has six beta-tubulin genes (*tbb-1*, *tbb-2*, *mec-7*, *tbb-4*, *ben-1*, and *tbb-6*) [25]. Of the six *C. elegans* beta-tubulins, MEC-7, TBB-4, and BEN-1 contain a phenylalanine at position 200, the residue hypothesized to bind BZs in *H. contortus* [18] and predicted to be BZ-sensitive. By contrast, TBB-1 and TBB-2 contain tyrosine at position 200 and are not predicted to bind BZs. Critically, *tbb-1* and *tbb-2* are the most broadly and highly expressed beta-tubulin genes in *C. elegans* and act redundantly for viability [26–28] as well as for movement, body morphology, and growth [29]. These data suggest that the essential microtubule pool comprises BZ-resistant isoforms (*tbb-1* and *tbb-2*). Therefore, BZ exposure delays development by its effects on BZ-sensitive isoforms (*ben-1*, *mec-7*, and *tbb-4*). Among the BZ-binding isoforms, *Cel*-BEN-1, an ortholog of *H. contortus tbb-isotype-1* and *tbb-isotype-2* [18], is the primary mediator of BZ response [30]. The third most highly expressed beta-tubulin, *ben-1*, is largely restricted to neurons, specifically cholinergic and glutamatergic neurons [25,31]. Although *ben-1* is not essential for survival, cell-specific rescue experiments demonstrated that *ben-1* acts in cholinergic and GABAergic neurons to confer BZ susceptibility, suggesting that these neurons are key sites of BZ action [31]. Additionally, a heterogeneous set of LoF variants in *ben-1* identified in *C. elegans* wild strains cause natural BZ resistance in this species [14]. The ability to maintain wild-type growth despite the loss of *ben-1* is likely explained by functional redundancy among beta-tubulin genes [32]. Together, these findings illustrate how loss of a *C. elegans* beta-tubulin that can bind BZs causes resistance because other beta-tubulin genes are functionally redundant for viability and do not bind BZs.

The recurrent association of beta-tubulin variants with BZ resistance in clade V parasitic and free-living nematodes suggests the hypothesis that resistance might be predictable across species. However, the reliability of beta-tubulin variants as predictors of BZ resistance across nematode species is unknown. This hypothesis is difficult to test directly in parasitic nematode species because of their host-dependent life cycles, poorly annotated reference genomes, and limited molecular and genetic tools [33,34]. By contrast, the availability of high-quality genomic data for hundreds of wild strains [35] and the laboratory tractability of the free-living *Caenorhabditis* nematode species, *C. elegans*, *Caenorhabditis briggsae*, and *Caenorhabditis tropicalis*, provide an opportunity to test predictions of beta-tubulin mediated BZ resistance in the *Caenorhabditis* genus. Establishing and interrogating patterns of repeated evolution in these three free-living species would provide a mechanistic framework to anticipate resistance-associated variants in beta-tubulin genes across other clade V nematode species, including parasitic nematodes where direct experimental validation of resistance mechanisms remains a challenge.

Using the global natural diversity of *C. elegans*, *C. briggsae*, and *C. tropicalis*, we assessed variation in the beta-tubulin genes *tbb-1*, *tbb-2*, *mec-7*, *tbb-4*, and *ben-1* and identified high-impact variants (*i.e.*, single nucleotide variants (SNVs), small insertions or deletions (INDELs), and structural variants (SVs)) predicted to disrupt beta-tubulin function and confer BZ resistance. Because *ben-1* is the primary driver of BZ resistance in *C. elegans*, we used an established high-throughput larval development assay (HTLDA) to expose strains with novel *ben-1* variants to the highly used BZ, albendazole (ABZ). In *C. elegans*, strains harboring seven of nine novel *Cel-ben-1* variants were resistant to ABZ, adding more alleles hypothesized to confer resistance in this species. By contrast, strains harboring only two of the eight unique *Cbr-ben-1* variants (W21stop and Q134H) were resistant to ABZ. *C. tropicalis* was distinct from the other two species, where no strains with variants in *ben-1* were resistant to ABZ. To validate the roles of *Cbr-ben-1* and *Ctr-ben-1* in BZ resistance, we generated deletion alleles and confirmed that loss of *ben-1* confers resistance in both *C. briggsae* and

C. tropicalis. Fecundity assays showed that a loss of *Cbr-ben-1* did not affect *C. briggsae* fitness, whereas a deletion of *Ctr-ben-1* significantly reduced fecundity in *C. tropicalis*. Because *ben-1* variants could not always predict ABZ resistance, we tested whether strains harboring high-impact variants in the other four conserved beta-tubulin genes were resistant to ABZ. Strains with variants in *tbb-1*, *tbb-2*, *mec-7*, and *tbb-4* were not resistant to ABZ in any of the three *Caenorhabditis* species, indicating that *ben-1* is the primary beta-tubulin that confers resistance. The species-specific patterns of beta-tubulin-mediated BZ resistance might reflect species-specific selection pressures, such as exposure to natural BZs, and can shape the evolution of beta-tubulin-mediated resistance. The identification of alleles associated with BZ resistance in experimentally tractable species establishes a framework to predict beta-tubulin variants associated with resistance in other clade V nematodes.

Results

Strains with variants or expression differences in *ben-1* were predicted to be ABZ resistant

To predict ABZ resistant strains in the three *Caenorhabditis* species, we identified high-impact variants (SNVs, INDELs, or SVs predicted to disrupt beta-tubulin function) in ben-1 (see Materials and Methods). In a set of 611 C. *elegans* wild strains [35], we identified 65 strains (10.6% of all strains) with 33 unique high-impact variants in *ben-1* (**S1 Table**). Of the 33 variants, 24 were previously phenotyped and 20 were associated with ABZ resistance (**S1A Fig**) [14,36]. In 641 *C. briggsae* wild strains, 22 strains (3.43% of all strains) with eight unique high-impact variants in *ben-1* were identified (**S2 Table**). In a set of 518 *C. tropicalis* wild strains, only two strains (0.39% of all strains) with unique high-impact variants in *ben-1* were identified (**S3 Table**).

Next, because low *ben-1* expression was previously correlated with ABZ resistance in *C. elegans* wild strains [37], we evaluated whether *ben-1* expression levels were predictive of ABZ responses in *C. elegans.* We assessed the relationship between the expression of *ben-1* [37] and ABZ responses in 180 *C. elegans* wild strains [14, 36] (p-value = 5.16e-16, $r^2 = 0.344$). We hypothesized that low *ben-1* expression could contribute to ABZ resistance in *C. briggsae* and *C. tropicalis*, but expression data from wild strains in these species have yet to be collected.

Altogether, we identified nine novel variants in *Cel-ben-1* (E3stop, Y50C, P80S, VDN113N, Q131L, frameshift 319, frameshift 368, stop445S, and a duplication) (**S1 Table**), one strain with low *Cel-ben-1* expression, eight variants in *Cbr-ben-1* (W21stop, V91I, Q94K, D128E, Q134H, S218L, M299V, and R359H) (**S2 Table**), and two variants in *Ctr-ben-1* (P80T and R121Q) (**S3 Table**) to test for ABZ resistance. In addition to these selected strains, we also selected *C. briggsae* and *C. tropicalis* strains that lacked high-impact variants in beta-tubulin genes but were closely related to strains with variants (S2, S3 Figs**, and S4 Table**). The strains with no high-impact variants in any beta-tubulin gene might control for differences in wild strain genetic backgrounds.

High-throughput larval development assays (HTLDAs) reveal species-specific associations between *ben-1* variation and ABZ resistance

Nematodes grow longer as they progress through development, and BZs slow this progression [14–16,32,36]. A longer animal length (*i.e.*, larger animals) corresponds to increased ABZ resistance, and a shorter animal length (*i.e.*, smaller animals) corresponds to increased ABZ sensitivity. To evaluate the effects of ABZ on animal length (a proxy for development), we used image-based HTLDAs to expose all *C. elegans*, *C. briggsae*, and *C. tropicalis* wild strains with novel high-impact variants in *ben-1* or low *ben-1* expression (*i.e.*, predicted resistant strains) to control (DMSO) (S4, S5, and **S6 Figs**) and drug (ABZ) conditions (**S7**, **S8, and S9 Figs**) (see *Materials and Methods*). The assay included 48 replicates per strain with five to 30 animals per replicate in DMSO or ABZ conditions. In DMSO conditions, strains naturally varied in animal length, but all animal measurements were categorized as the L4 larval stage by our custom *CellProfiler* models [38,39], indicating all strains underwent normal development in control conditions. In ABZ conditions, the

reported nematode length (*i.e.*, normalized animal length (μm)) of each strain is the difference between animal lengths in DMSO and ABZ.

To define the role of *ben-1* in BZ response and classify wild strains as BZ resistant, we first obtained or created *ben-1* deletions in the reference strains for each of the three *Caenorhabditis* species. In *C. elegans*, the strain with a *ben-1* LoF variant in the N2 strain background (ECA882) has been used as an ABZ-resistant control previously [14,32,36]. For *C. briggsae* and *C. tropicalis*, we used CRISPR-Cas9 genome editing to generate two independent *ben-1* deletion alleles per species (see *Materials and Methods*). In *C. briggsae*, deletions of *Cbr-ben-1* were created in the AF16 reference strain background (ECA3953 and ECA3954) (**S10 Fig and S5 Table**). In *C. tropicalis*, deletions of *Ctr-ben-1* were created in the NIC58 reference strain background (ECA4247 and ECA4248) (**S11 Fig and S5 Table**). All deletions of *ben-1* in each of the three *Caenorhabditis* species conferred high levels of ABZ resistance (**S12 and S13 Figs**). Wild strains were then classified as resistant using a threshold where the median animal lengths after ABZ exposure were no more than two SD below the median animal length of the species-specific *ben-1* deletion strain.

In *C. elegans*, seven of the nine strains with *ben-1* variants showed minimal developmental delays after exposure to ABZ, a phenotype similar to loss of *ben-1*, and were classified as resistant (**Fig 1**). The two remaining strains with *ben-1* variants (P80S and stop445S) and the strain with low *ben-1* expression were not strongly resistant to ABZ. The P80S variant might partially alter *ben-1* function, causing a moderate resistance phenotype. In stop445S, the normal stop

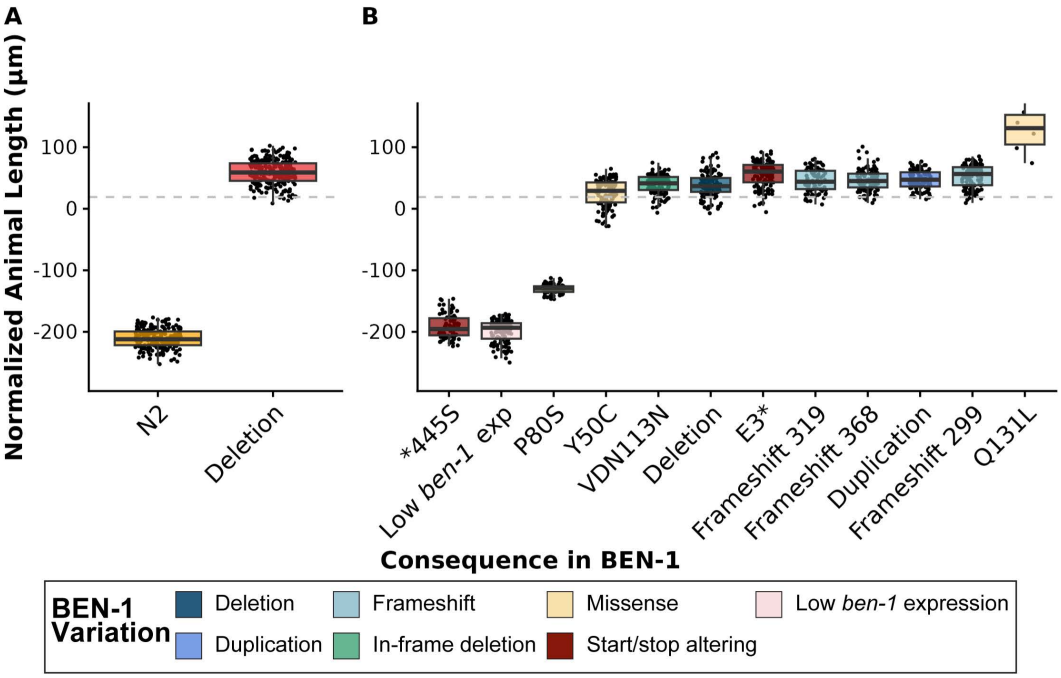

Fig 1. High-throughput larval development assays in the presence of albendazole for *C. elegans* strains with unique high-impact variants in BEN-1. The regressed median animal length values for populations of nematodes grown in 30 μM albendazole (ABZ) are shown on the y-axis. Each point represents the normalized median animal length value (*i.e.*, the difference between animal lengths in DMSO and ABZ for each strain) of a well containing approximately five to 30 animals. Data are shown as Tukey box plots with the median as a solid horizontal line, and the top and bottom of the box representing the 75th and 25th quartiles, respectively. The top whisker is extended to the maximum point that is within the 1.5 interquartile range from the 75th quartile. The bottom whisker is extended to the minimum point that is within the 1.5 interquartile range from the 25th quartile. The gray dashed line marks the *C. elegans* resistance threshold, defined as two standard deviations below the mean of the *ben-1* deletion strain in the N2 reference strain background. Results for **(A)** the N2 reference strain (orange) and a strain with a *ben-1* deletion in the N2 background (red), and **(B)** all wild *C. elegans* strains with unique high-impact variants in *ben-1* are sorted by their relative resistance to ABZ based on median animal length. Wild *C. elegans* strains are colored by beta-tubulin variant status. An asterisk indicates a stop gained at the indicated BEN-1 position.

https://doi.org/10.1371/journal.ppat.1014306.g001

codon was replaced with a serine. This variant likely does not affect *ben-1* function because position 445 is at the end of the BEN-1 protein, and only four amino acid residues (NRKL) are added beyond the wild-type stop codon. Finally, the strain with low *ben-1* expression and no high-impact variants in *ben-1* (JU1581) was sensitive to ABZ, indicating that the selected threshold of *ben-1* expression (≥3.75 TPM) still retained strains with adequate *ben-1* function. Overall, natural allelic variation in *Cel-ben-1* is associated with BZ resistance, recapitulating previous findings that BZ resistance is associated with a diverse set of LoF variants in *Cel-ben-1* [14,29,32,36].

In *C. briggsae*, we performed HTLDAs on the AF16 reference strain (ABZ sensitive), two *ben-1* deletion strains (ECA3953 and ECA3954) (ABZ resistant), 11 strains with eight unique variants in *ben-1*, and 13 strains genetically related to strains with *ben-1* variants in DMSO (control) (**S5 Fig**) and ABZ conditions (**Figs 2**, **S8 and S12**). Of the 11 strains with *Cbr-ben-1* variants, only two strains with unique variants in BEN-1 (Q134H and W21stop) were ABZ resistant (**Fig 2**). The Q134H amino acid change has been associated with ABZ resistance in *A. caninum* and validated in *C. elegans* [11]. An early stop gain at position 21 is predicted to cause the premature termination of protein synthesis and LoF. Of all the assayed strains with variants in BEN-1, six (V91I, Q94K, D128E, S218L, M299V, and R359H) were not resistant to ABZ. Additionally, eleven *C. briggsae* strains were exposed to a maximum concentration of 120 μM ABZ, where only two strains with the variants Q134H and W21stop were resistant at these higher concentrations (**Fig 3**). Overall, because only one of the seven missense variants was associated with ABZ resistance, we could not reliably predict *C. briggsae* ABZ

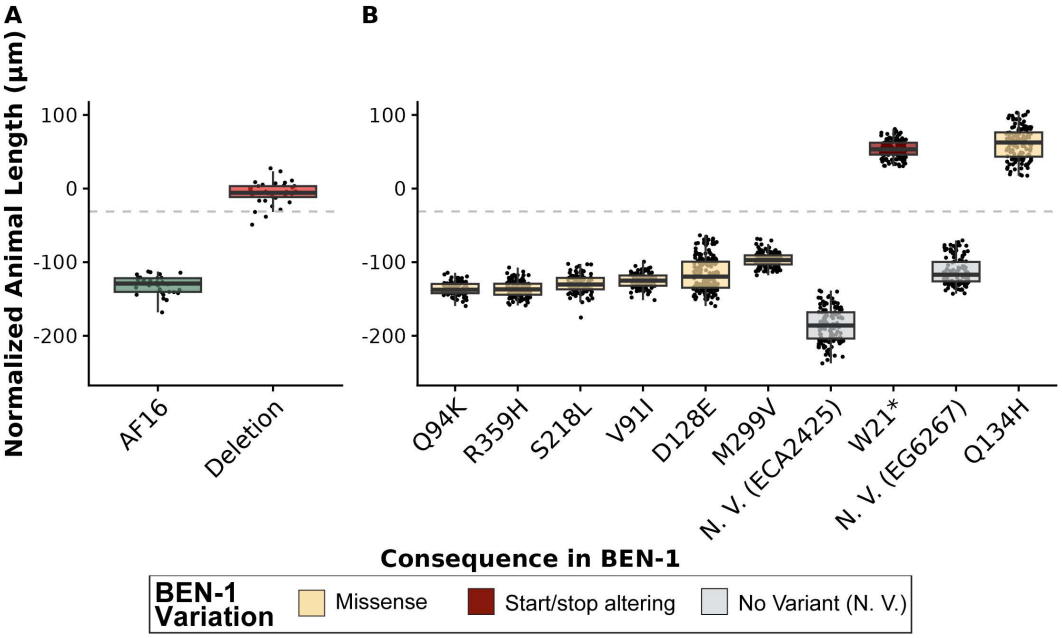

Fig 2. High-throughput larval development assays in the presence of albendazole for *C. briggsae* strains with unique high-impact variants in BEN-1. The regressed median animal length values for populations of nematodes grown in 30 μM albendazole (ABZ) are shown on the y-axis. Each point represents the normalized median animal length value of a well containing approximately five to 30 animals. Data are shown as Tukey box plots with the median as a solid horizontal line, and the top and bottom of the box representing the 75th and 25th quartiles, respectively. The top whisker is extended to the maximum point that is within the 1.5 interquartile range from the 75th quartile. The bottom whisker is extended to the minimum point that is within the 1.5 interquartile range from the 25th quartile. The gray dashed line marks the *C. briggsae* resistance threshold, defined as two standard deviations below the mean of the *ben-1* deletion strain in the AF16 reference strain background. Results for **(A)** the AF16 reference strain (green) and a strain with a *ben-1* deletion in the AF16 background (red), and **(B)** all wild *C. briggsae* strains with unique high-impact variants in *ben-1* are sorted by their relative resistance to ABZ based on median animal length. No variant (N. V.) strains (gray) paired with strains that have a high-impact variant in *ben-1* that pass the resistance threshold are shown alongside each corresponding strain with a high-impact variant in *ben-1*. Wild *C. briggsae* strains are colored by beta-tubulin variant status.

https://doi.org/10.1371/journal.ppat.1014306.g002

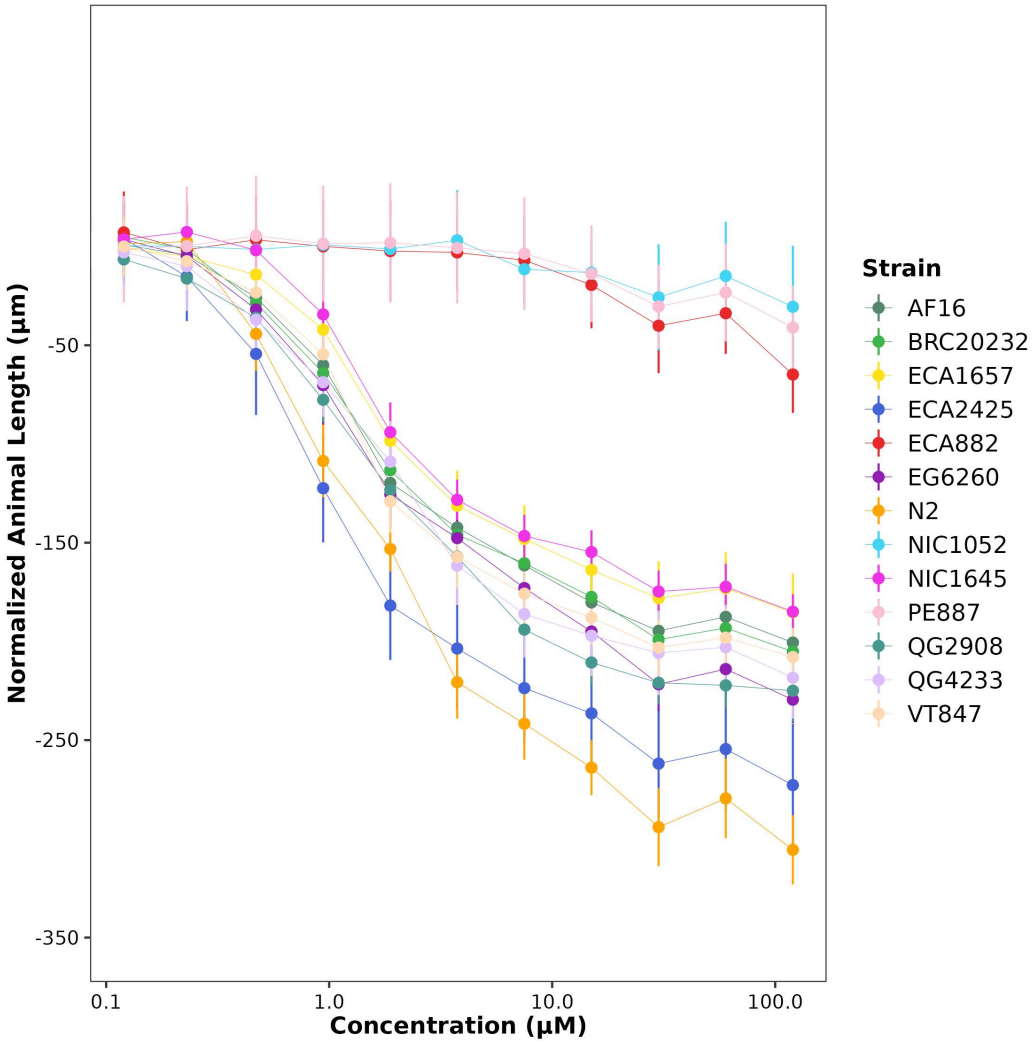

Fig 3. Dose-response curves for *C. briggsae* strains in albendazole. Normalized animal lengths (y-axis) are plotted for each strain as a function of the dose of albendazole (ABZ) in the high-throughput larval development assay (HTLDA) (x-axis). Strains are denoted by color. Lines extending vertically from points represent the standard deviation from the mean response. Statistical normalization of animal lengths is described in *Materials and Methods*. *C. elegans* strains N2 and ECA882 were added for ABZ-susceptible and ABZ-resistant controls, respectively.

https://doi.org/10.1371/journal.ppat.1014306.g003

resistance based on the presence of a missense variant alone. To evaluate the potential fitness consequences of *ben-1* LoF alleles, fecundity assays were performed between the AF16 reference strain and the two strains with a loss of *ben-1* in the AF16 background (ECA3953 and ECA3954) (**Fig 4A and S6 Table**). We found no significant differences in fecundity between the three strains, indicating that a loss of *ben-1* does not affect fitness in this species. Similar results have been reported in *C. elegans*, where loss of *Cel-ben-1* has no effect on fitness [36]. These results indicate that, although a loss of *Cbr-ben-1* confers ABZ resistance with no fitness detriment, ABZ resistance associated with *Cbr-ben-1* variants is uncommon.

In *C. tropicalis*, we performed HTLDAs on the reference strain NIC58 (ABZ sensitive), two independent deletions of *Ctr-ben-1* (ECA4247 and ECA4248) (ABZ resistant), two *C. tropicalis* strains with variants in *ben-1* (P80T and R121Q), and two strains genetically related to *ben-1* variant strains in DMSO (**S6 Fig**) and ABZ conditions (**Figs 5 and S9**). We

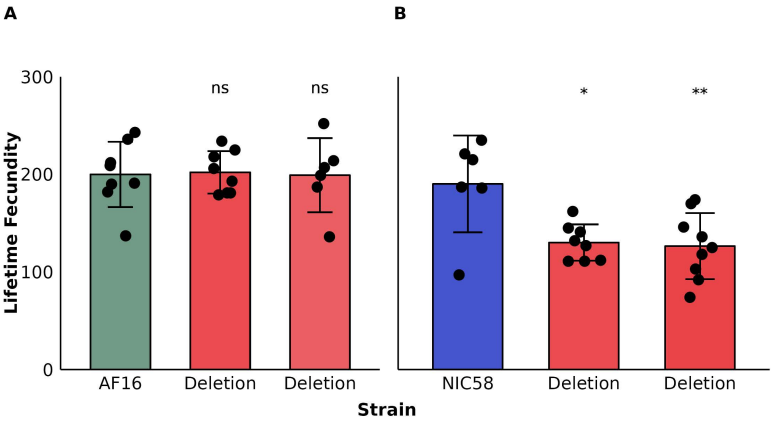

Fig 4. Variation in lifetime fecundity between the *C. briggsae* (AF16) and *C. tropicalis* (NIC58) reference strains and strains with a loss of *ben-1* in the AF16 and NIC58 reference strain backgrounds. Bar plots for the lifetime fecundity, y-axis, for each strain on the x-axis are shown. Error bars show the standard deviation of lifetime fecundity among six to nine replicates. **(A)** A comparison of lifetime fecundities between the *C. briggsae* laboratory reference strain AF16 (green) and the two independently edited *C. briggsae* AF16 strains with a loss of *ben-1* (red). **(B)** A comparison between the *C. tropicalis* laboratory reference strain NIC58 (blue) and two independently edited *C. tropicalis* NIC58 strains with a loss of *ben-1* (red). Statistical significance was determined using Tukey HSD. Significance of each comparison is shown above each comparison pair ($p > 0.05$ = ns, $p < 0.05$ = *, $p < 0.01$ = **, Tukey HSD).

https://doi.org/10.1371/journal.ppat.1014306.g004

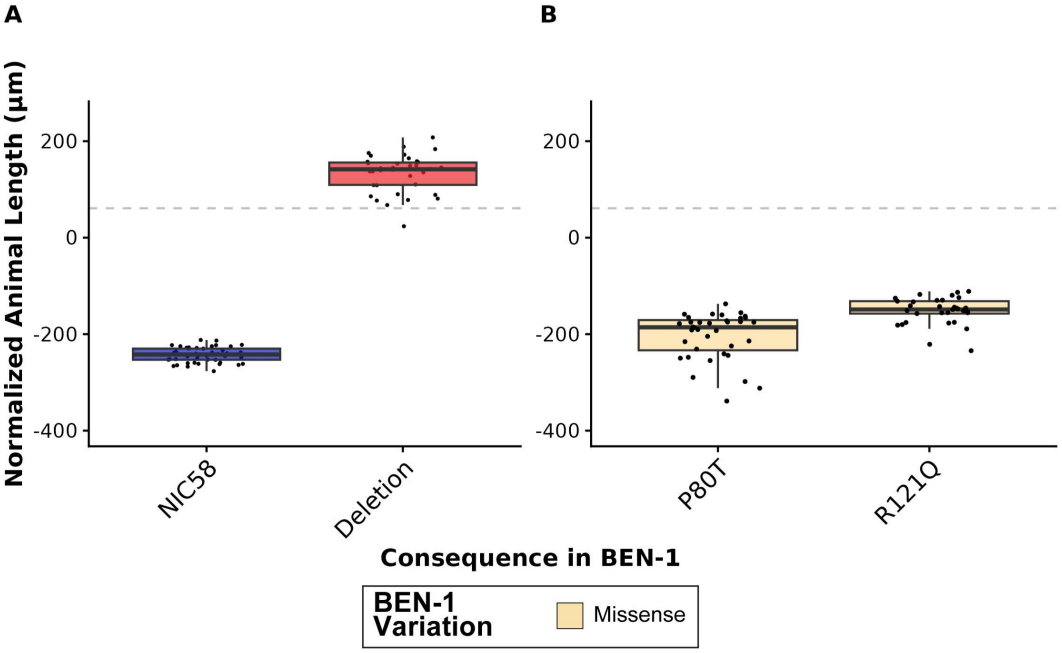

Fig 5. High-throughput larval development assays in the presence of albendazole for *C. tropicalis* strains with unique high-impact variants in BEN-1. The regressed median animal length values for populations of nematodes grown in 30 μM albendazole (ABZ) are shown on the y-axis. Each point represents the normalized median animal length value of a well containing approximately five to 30 animals. Data are shown as Tukey box plots with the median as a solid horizontal line, and the top and bottom of the box representing the 75th and 25th quartiles, respectively. The top whisker is extended to the maximum point that is within the 1.5 interquartile range from the 75th quartile. The bottom whisker is extended to the minimum point that is within the 1.5 interquartile range from the 25th quartile. The gray dashed line marks the *C. tropicalis* resistance threshold, defined as two standard deviations below the mean of the *ben-1* deletion strain in the NIC58 reference strain background. Results for **(A)** the NIC58 reference strain (blue) and a strain with a *ben-1* deletion in the NIC58 background (red), and **(B)** all wild *C. tropicalis* strains with unique high-impact variants in *ben-1* are sorted by their relative resistance to ABZ based on median animal length. Wild *C. tropicalis* strains are colored by beta-tubulin variant status.

https://doi.org/10.1371/journal.ppat.1014306.g005

found that all *C. tropicalis* wild strains displayed ABZ sensitivity, indicating that P80T and R121Q are not associated with ABZ resistance (Fig 5). Additionally, all tested wild strains were exposed to a maximum concentration of 120 μM ABZ, and none of the strains displayed resistance at these higher concentrations (Fig 6). Finally, to evaluate the potential fitness consequences caused by a loss of *ben-1*, fecundity assays were performed between the NIC58 reference strain and the two strains with a loss of *ben-1* in the NIC58 background (ECA4247 and ECA4248) (**Fig 4B and S7 Table**). We found that a deletion of *ben-1* caused a significant reduction in fecundity in *C. tropicalis* (Fig 4B). The fitness defect caused by a loss of *ben-1* could explain the absence of naturally occurring *ben-1* variants in wild *C. tropicalis* strains, suggesting that *C. tropicalis* is unlikely to acquire natural *ben-1* variants that confer ABZ resistance without strong selection. If ABZ resistance is present in *C. tropicalis* wild strains, its genetic basis remains unknown and involves factors distinct from *ben-1*. Lastly,

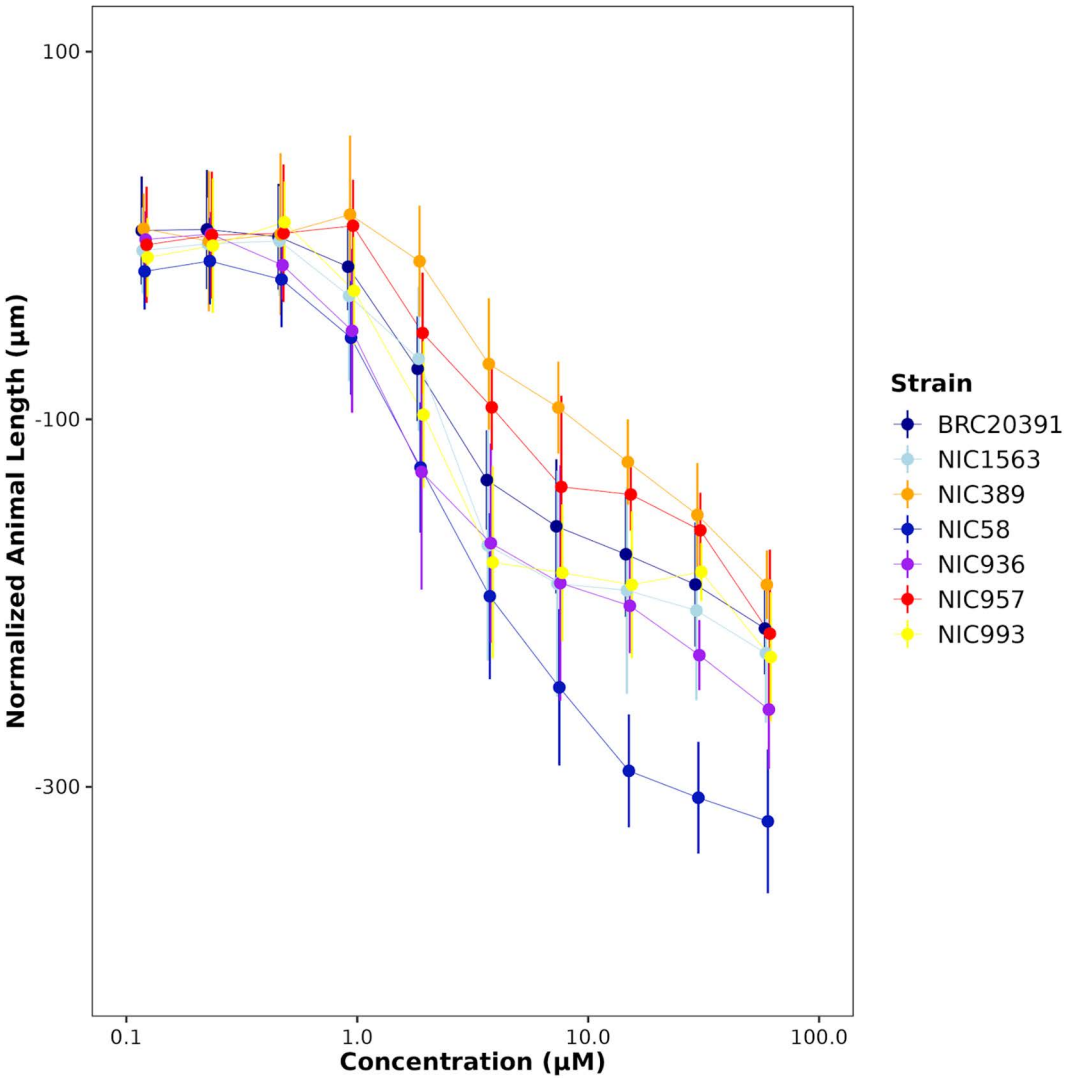

Fig 6. Dose-response curves for *C. tropicalis* strains in albendazole. Normalized animal lengths (y-axis) are plotted for each strain as a function of the dose of albendazole (ABZ) in the high-throughput larval development assay (HTLDA) (x-axis). Strains are denoted by color. Lines extending vertically from points represent the standard deviation from the mean response. Statistical normalization of animal lengths is described in *Materials and Methods*.

https://doi.org/10.1371/journal.ppat.1014306.g006

we only tested the effects of ABZ, testing another BZ analog would be necessary to determine whether the observed patterns of resistance are consistent throughout the BZ drug class.

Resistance-associated *ben-1* variants are located within the protein core near the predicted BZ-binding site

To evaluate whether the predicted molecular consequence and severity of *ben-1* variants were predictive of BZ resistance, we characterized the identities and predicted functional impacts of each amino acid altering variant. We distinguished between alleles that disrupt multiple amino acids (*i.e.*, frameshifts, stop/start altering variants, and SVs) and alleles that affect a single amino acid (*i.e.*, missense alleles). Multi-site alleles were excluded from further analysis because they are predicted to severely disrupt or terminate BEN-1 function, whereas missense alleles might preserve an intact protein and allow interpretation of residue-level effects on BZ interaction.

In *C. elegans*, seven unique missense substitutions in BEN-1 were identified, of which five (Y50C, Q131L, S145F, A185P, M275I) were associated with BZ resistance (**S7 Fig**) [14]. In *C. briggsae*, seven unique missense substitutions in *Cbr*-BEN-1 were identified, but only Q134H was associated with BZ resistance (**S8 Fig**). In *C. tropicalis*, both missense substitutions (P80T and R121Q) were not associated with BZ resistance (**S9 Fig**). To evaluate if missense variants with larger predicted functional impacts were associated with BZ resistance, we quantified the severity of each substitution using BLOSUM62 and Grantham scores [40,41]. BLOSUM scores measure the evolutionary likelihood of observing a specific missense substitution, and Grantham scores measure the physicochemical severity of a substitution. We reasoned that missense substitutions that confer BZ resistance would either disrupt BEN-1 function or affect BZ binding. In both cases, substitutions predicted to be more structurally disruptive or evolutionarily less tolerated should be enriched among resistance-associated alleles. Because *C. elegans* had the most missense variants associated with BZ resistance, we performed a regression analysis of each strain's response to ABZ by the BLOSUM or Grantham scores of the strain's beta-tubulin variant. For *C. elegans*, neither BLOSUM nor Grantham scores showed a significant correlation with ABZ response (**S14 Fig**). By contrast, too few missense variants were associated with BZ resistance among *C. briggsae* and *C. tropicalis* strains to meaningfully interpret BLOSUM or Grantham scores for these species (**S8 Table**). The limited number of missense substitutions among wild strains and the even smaller subset associated with BZ resistance constrained statistical power to evaluate structure-function relationships between naturally occurring beta-tubulin variants and BZ response.

To complement the sequence-based analysis, we evaluated the structural position of each variant relative to the predicted BZ-binding site. We mapped missense variants onto an AlphaFold-predicted BEN-1 protein structure that showed that the five *C. elegans* missense substitutions associated with resistance are located within the core, whereas the two substitutions not associated with resistance (P80S and D404N) are on the protein surface (**Fig 7A**). By contrast, all *C. briggsae* (except Q134H) and all *C. tropicalis* missense substitutions are on the protein surface and are not associated with resistance (**Fig 7B and 7C**). For structural comparison, we modeled *H. contortus tbb-isotype-1* beta-tubulin bound to ABZ, and highlighted the canonical missense variants at positions 167, 198, and 200 (**Fig 7D**), all of which are located within the core of the structure, near the predicted BZ-binding pocket and are associated with resistance [18–22,42]. These results suggest that BZ resistance is associated with missense substitutions occurring within the protein core likely affecting the theoretical BZ-binding pocket.

Natural variants in *tbb-1*, *tbb-2*, *mec-7*, and *tbb-4* are not associated with ABZ resistance across the three free-living *Caenorhabditis* species

Although it has been established that *ben-1* is the primary gene involved in ABZ resistance in *C. elegans* [14,32,36], we know less about the role each beta-tubulin gene plays in *C. briggsae* and *C. tropicalis* ABZ resistance. Therefore, we identified variants in the other four conserved beta-tubulin genes across the three *Caenorhabditis* species. We found no variants in *Cel-tbb-1* or *Cel-tbb-2* in any *C. elegans* wild strains (CaeNDR Release ID: *C. elegans* - 20231213) (**Fig 8**). However, we did identify strains with one missense variant (A9T) in *Cel-mec-7*, a splice donor variant in *Cel-mec-7*, or

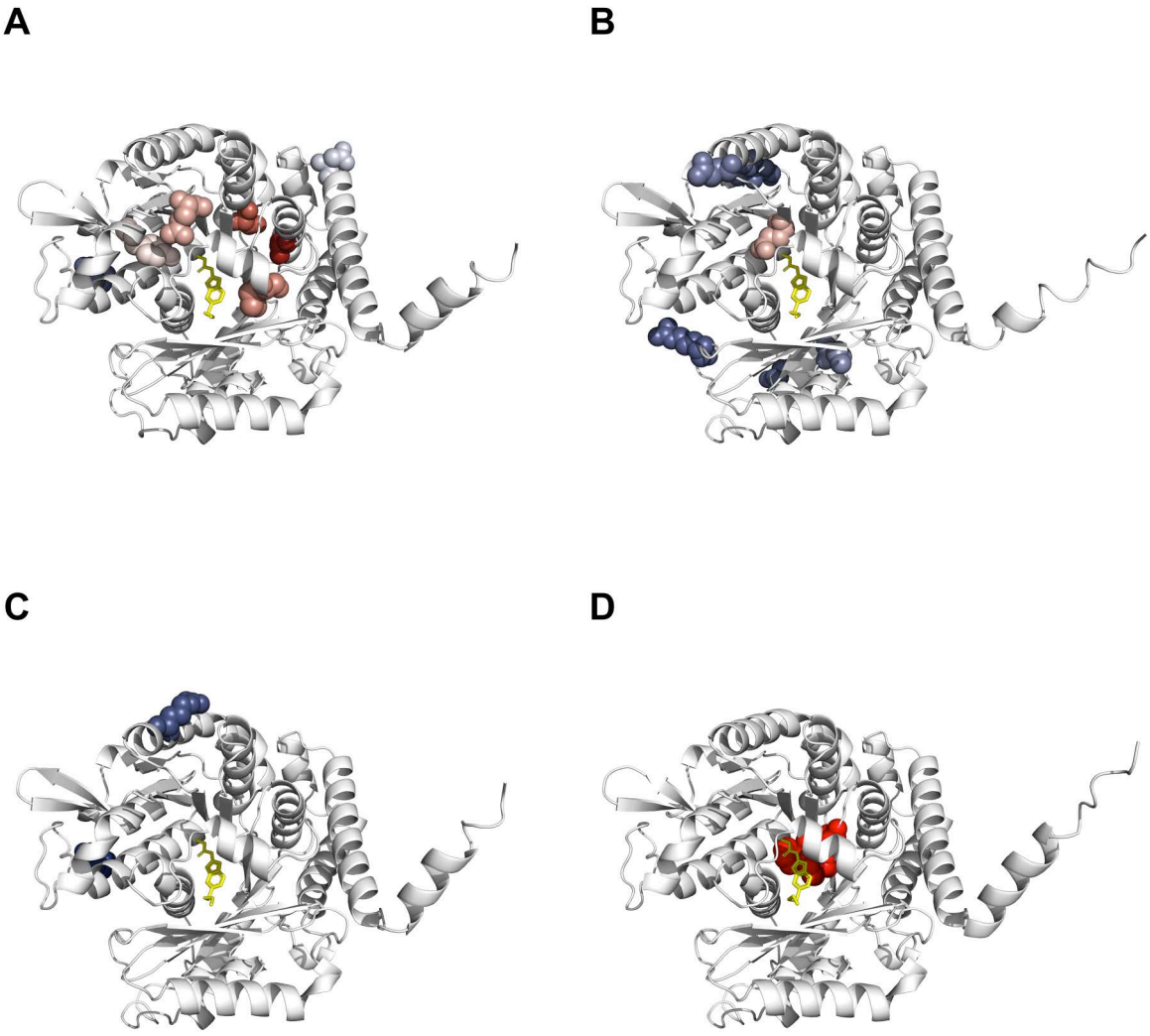

Fig 7. Structure of beta-tubulin orthologs bound to albendazole. AlphaFold3 models of BEN-1 orthologs bound to albendazole (ABZ) are shown for **(A)** *Cel*-BEN-1, **(B)** *Cbr*-BEN-1, **(C)** *Ctr*-BEN-1, and **(D)** *Hcon*-TBB-ISO-1. ABZ is colored yellow. Residues impacted by amino acid substitutions are colored by resistance (red) or sensitivity (blue).

https://doi.org/10.1371/journal.ppat.1014306.g007

one missense variant in *Cel-tbb-4* (Q8H) (**S1 Table**). The strain with a splice donor variant in *Cel-mec-7* also carried a high-impact variant (*445S) in *Cel-ben-1*. We also assessed the relationship between the expression of *Cel-tbb-1*, *Cel-tbb-2*, *Cel-mec-7*, or *Cel-tbb-4* [37] and ABZ responses in 180 wild strains (**S15 Fig**) [14,36]. In *C. briggsae*, we identified strains with missense variants in *Cbr-tbb-1* (T35A, V64I, A275T, and L377I), *Cbr-tbb-2* (E441A), *Cbr-tbb-4* (A271V), and *Cbr-mec-7* (T136I, N165S, and S338C) (CaeNDR Release ID: *C. briggsae* - 20240129) (**S2 Table**). In *C. tropicalis*, we identified no high-impact variants in *Ctr-tbb-1*, one missense variant in *Ctr-tbb-2* (N89S), two missense variants in *Ctr-mec-7* (P80F, D433E), and one missense variant in *Ctr-tbb-4* (A78V) (CaeNDR Release ID: *C. tropicalis* - 20231201) (**S3 Table**). Because expression data from *C. briggsae* and *C. tropicalis* wild strains have yet to be collected, we could not test correlations of beta-tubulin gene expression with resistance. We performed HTLDAs under control (DMSO) (S16, S17, **and S18 Figs**) and ABZ conditions (**S19**, **S20 and S21 Figs**) on strains in the three *Caenorhabditis* species carrying variants in the conserved beta-tubulin genes *tbb-1*, *tbb-2*, *mec-7*, and *tbb-4*, along with strains genetically related to strains

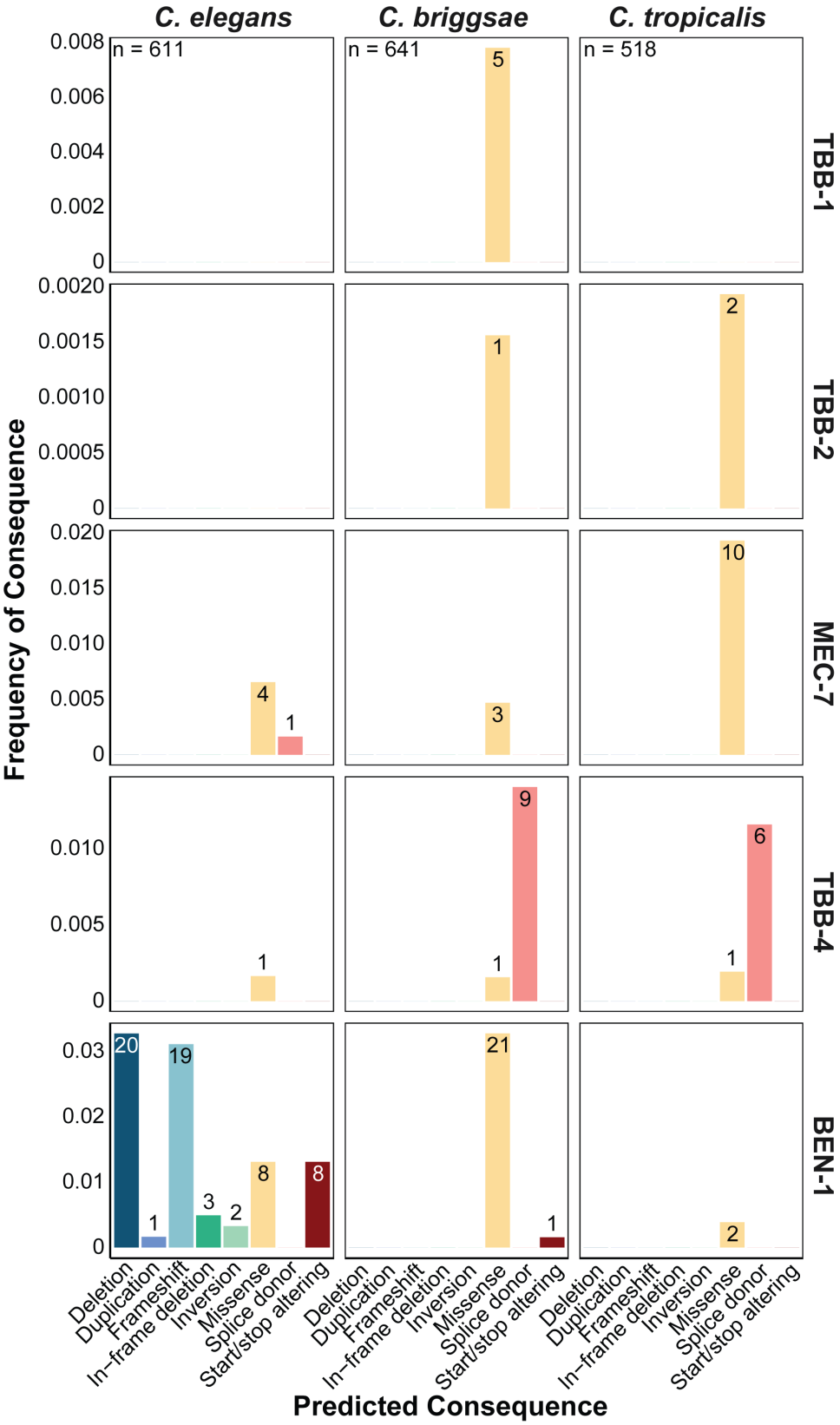

Fig 8. The frequency of predicted high-impact consequences in the five conserved beta-tubulin genes present in natural populations of *C. elegans*, *C. briggsae*, and *C. tropicalis*. The frequency of single nucleotide variants (SNVs) and structural variants (SVs) present in natural populations

of *C. elegans* (n = 611), *C. briggsae* (n = 641), and *C. tropicalis* (n = 518) (y-axis) are shown by their predicted consequence in each beta-tubulin gene (x-axis). The frequency of each consequence was calculated as the number of strains carrying a particular predicted consequence divided by the total number of strains sampled for each species. The total number of isotype reference strains with a given predicted consequence are displayed on top of each bar plot.

https://doi.org/10.1371/journal.ppat.1014306.g008

with variants in those beta-tubulin genes. No variants outside of *ben-1* conferred ABZ resistance in any species, indicating that natural missense variants in *tbb-1*, *tbb-2*, *mec-7*, and *tbb-4* are not associated with BZ resistance in the three selfing *Caenorhabditis* species.

Differences in tissue- and cell-specific expression patterns of beta-tubulins might influence BZ susceptibility

Tissue-specific differences in beta-tubulin expression among the three *Caenorhabditis* species could influence BZ resistance. To compare beta-tubulin expression patterns, we analyzed two whole-animal single-cell transcriptomic datasets that quantify gene expression patterns across *C. elegans*, *C. briggsae*, and *C. tropicalis* [44,45]. A comparison of embryonic gene expression levels in *C. elegans* and *C. briggsae* revealed that beta-tubulin gene expression during embryogenesis is highly conserved (**S9 and S10 Tables**). On average, the five beta-tubulin gene distances, which quantify expression conservation across homologous cell types, were small (mean beta-tubulin JSDgene = 0.29) (**S9 Table**) [43] and expression breadth across all cell types (*i.e.*, cell-type specificity) was conserved (**S10 Table**). Among beta-tubulin genes, *tbb-2* displayed the greatest divergence in embryonic gene expression breadth, the largest difference across species in cell-type specificity (**S10 Table**). Overall, embryonic beta-tubulin expression patterns are conserved between *C. elegans* and *C. briggsae*, although *tbb-2* expression breadth is an exception (**S10 Table**).

Next, because neuronal *ben-1* expression restores BZ susceptibility in *C. elegans* [31], we focused on the divergence of beta-tubulin expression across homologous neuronal cell classes at the L2 larval stage [43]. For each gene, we quantified neuron-class-specific expression divergence across the three *Caenorhabditis* species using the proportion of neuronal classes where gene expression differs (**S11 Table**) [43]. At least one species expressed *ben-1* in 98 of 118 neuronal cell classes. However, all three *Caenorhabditis* species expressed *ben-1* in only 35 of these classes (Jaccard distance = 0.64) (**S11 Table**). By contrast, *tbb-1* and *tbb-2* had highly conserved expression across the three *Caenorhabditis* species (98 of 118 neuronal cell classes expressed *tbb-1* or *tbb-2* in all three species) (Jaccard distance = 0) (**S11 Table**) [43]. The broad and conserved neuronal expression of *tbb-1* and *tbb-2* contrasts with *ben-1*, which showed narrower and species-specific expression patterns. Next, because *ben-1* expression in cholinergic neurons restores BZ susceptibility in *C. elegans* [43,44], we compared cholinergic neuronal expression and identified several cell classes with species-specific patterns. Generally, beta-tubulin cell specificity is conserved across the three *Caenorhabditis* species (**S9**, **S10, and S11 Tables**). However, examples of expression divergence among *C. elegans*, *C. briggsae*, and *C. tropicalis* were identified for *ben-1* and *tbb-2.* The divergence in *ben-1* expression across cholinergic cell classes indicates that the neuronal sites where *ben-1* function causes BZ susceptibility could differ among species. Future work should test this hypothesis using transgenic strains that express *ben-1* in different tissues and neuronal cells.

The most diverse high-impact variants are found in *Cel-ben-1*

To better understand the evolution of predicted BZ resistance alleles in the three *Caenorhabditis* species, we assessed the population-wide frequencies of each beta-tubulin variant. First, to determine the prevalence of high-impact variants in the five conserved beta-tubulin genes (*tbb-1*, *tbb-2*, *mec-7*, *tbb-4*, and *ben-1*) across *Caenorhabditis* species, we quantified the frequency of each consequence (deletion, duplication, frameshift, in-frame deletion, inversion, missense, splice donor, and start/stop altering) in each species. With global sampling of the three *Caenorhabditis* species (*C. elegans*: 611 strains, *C. briggsae*: 641 strains, *C. tropicalis*: 518 strains), we found that *C. elegans* variants predicted to cause

deleterious functional effects were present in 1% of strains. By contrast, variants predicted to cause deleterious functional effects in *C. briggsae* and *C. tropicalis* were rare (< 0.05% of all strains in either species) (**Fig 8**). The most variation in beta-tubulin genes was identified in *Cel-ben-1*, where deletions, frameshifts, in-frame deletions, inversions, missense, stop/start altering variants, and a duplication were found. Next, we found one missense variant in *Cel-tbb-4* and several missense variants and a splice donor in *Cel-mec-7*. Overall, *C. elegans* has acquired the most diverse set of high-impact variants and predicted functional effects on *ben-1*. In *C. briggsae*, we found 21 missense amino acid substitutions and a single start/stop altering consequence in *Cbr-ben-1*. In both *Cbr-tbb-1* and *Cbr-tbb-2*, we identified rare missense consequences. Additionally, we found nine strains with splice variants in *Cbr-tbb-4* and one strain with a missense variant. In *C. tropicalis*, we found missense consequences in all beta-tubulin genes, except *tbb-1*. Additionally, we found six strains with splice variants in *Ctr-tbb-4*. These findings highlight that *Cel-ben-1* has the most diverse set of variants, reinforcing its role in BZ resistance.

Next, we examined the geographic distribution of strains carrying high-impact variants in *tbb-1*, *tbb-2*, *mec-7*, *tbb-4*, and *ben-1* to determine if beta-tubulin variants were associated with natural sampling location. In *C. elegans*, variants in *ben-1* were found globally with no discernible geographic pattern but were concentrated in clades that have experienced recent selective sweeps [45,46] (Fig 9B). *Cel-ben-1* variants in swept clades suggest that these mutations arose as relatively recent evolutionary events in response to BZ-like compounds in the natural niche. By contrast, in *C. briggsae*, variants in *ben-1* were distributed throughout the species tree and found on more ancestral branches (*i.e.*, earlier diverged lineages in the species) (Fig 9C). For *C. tropicalis*, the limited number of variants in *ben-1* precludes any definitive conclusions regarding their evolutionary patterns (Fig 9D). Because few variants are found in *tbb-1* (S22 Fig), *tbb-2* (S23 Fig), *mec-7* (S24 Fig), and *tbb-4* (S25 Fig), we cannot identify the evolutionary patterns of BZ resistance in these genes for any of the three species.

Finally, because substrates harbor distinct microbial communities that can influence the evolution of BZ resistance alleles, we determined if strains carrying a high-impact variant in a beta-tubulin gene were associated with specific substrates. Substrate categories were obtained from CaeNDR collection metadata and were classified into 12 major substrates (*i.e.*, arthropod, bait, compost, fungus, mollusk, moss, rotting flower, rotting nut, rotting stem, rotting wood, soil, or vegetal litter) [35,47,48]. A substrate enrichment analysis was performed to assess correlations between 12 substrates and all strains in the three *Caenorhabditis* species (**S12 Table**). However, no significant enrichment was observed between a high-impact variant in a beta-tubulin gene and any given substrate (Fisher's Exact Test, $p = 1$) (**S26Fig**). Because no geographic or substrate enrichment was observed, evolutionary pressures driving beta-tubulin variation are likely not strongly tied to substrate. However, our broad substrate categories and small number of BZ resistant *C. briggsae* and *C. tropicalis* strains might obscure finer-scale ecological patterns. Future studies characterizing microbial communities associated with each substrate might clarify the selective pressures on *Caenorhabditis* nematodes.

Discussion

Beta-tubulin-mediated BZ resistance varies across natural populations of *Caenorhabditis* nematodes

This study provides new insights into beta-tubulin-mediated ABZ resistance across three *Caenorhabditis* species. Each *Caenorhabditis* species harbored a unique set of predicted high-impact beta-tubulin alleles, but only variants in *ben-1* conferred resistance. With additional wild strains since our first study, we identified more *Cel-ben-1* LoF alleles associated with BZ resistance, which confirmed that a diverse collection of predicted LoF variants in *ben-1* are associated with ABZ resistance in *C. elegans* [14, 16]. In *C. briggsae*, strains harboring only two of the eight unique *Cbr-ben-1* variants were resistant to ABZ. One *Cbr-ben-1* variant (W21stop) causes early protein termination, and the other (Q134H) alters a residue within the *Cbr*-BEN-1 protein that likely affects ABZ binding and is associated with resistance in *A. caninum* [11]. A CRISPR-Cas9-generated deletion of *Cbr-ben-1* conferred resistance similar to that displayed by wild strains with these alleles and did not impact fitness. To date, resistance has yet to be identified in *C. tropicalis* wild strains. However, a

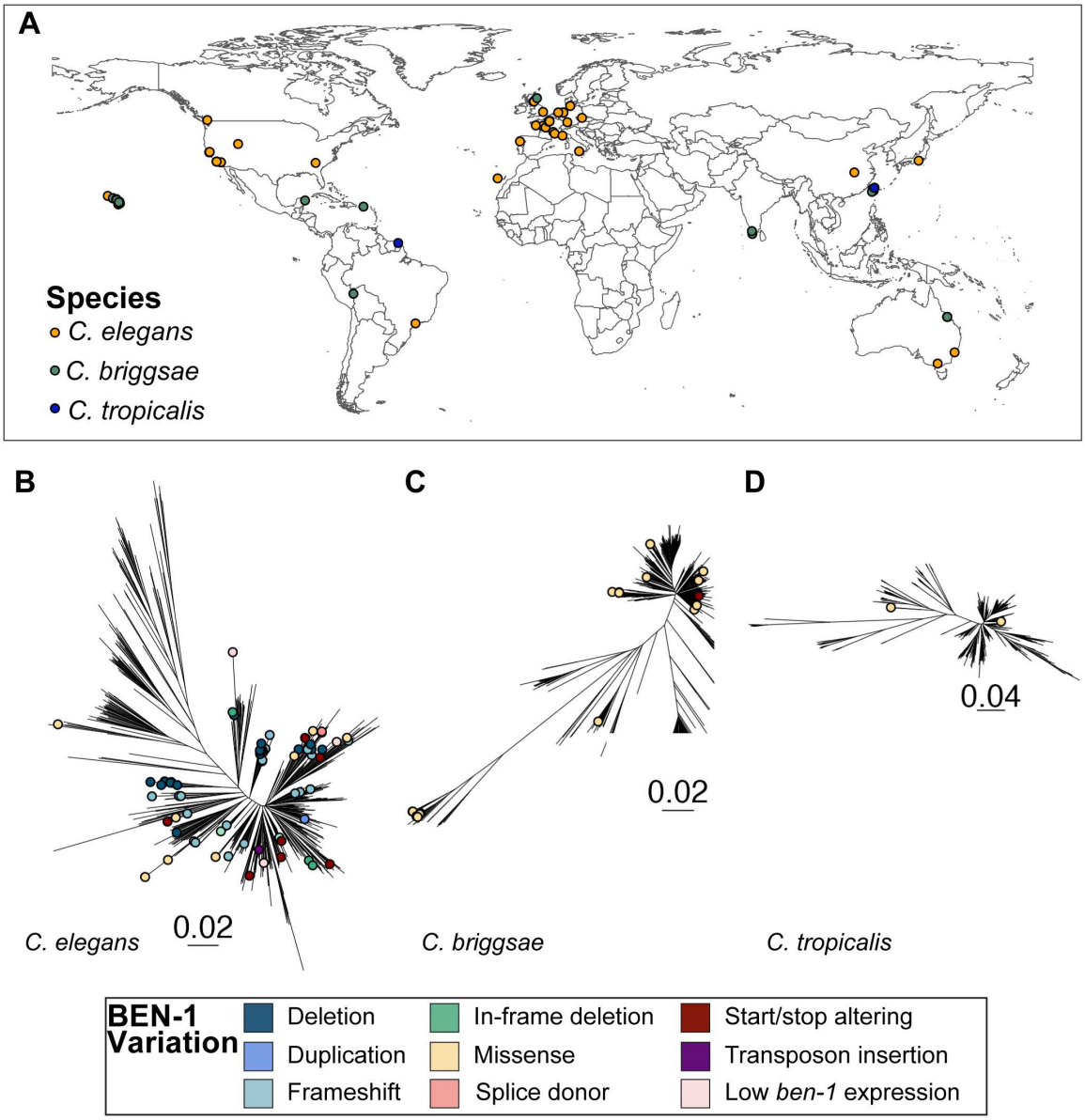

Fig 9. The global distribution of *Caenorhabditis* strains that contain predicted high-impact variation in BEN-1. (A) Each point corresponds to the sampling location of an individual *C. elegans* (orange), *C. briggsae* (green), or *C. tropicalis* (blue) isotype reference strain with a predicted high-impact consequence in BEN-1. A genome-wide phylogeny of **(B)** 611 *C. elegans*, **(C)** 641 *C. briggsae*, and **(D)** 518 *C. tropicalis* isotype reference strains, where each point denotes an isotype reference strain with a predicted high-impact consequence in BEN-1 is shown. The base layer of the map was obtained from the Natural Earth world countries shape file accessed via the *R* package *maturalearth* and function *ne_countries()*. The scale was set to return a medium-scale base map with the *scale = medium* parameter. The direct link to the base layer of the map can be accessed here: https://www.naturalearth-data.com/.

https://doi.org/10.1371/journal.ppat.1014306.g009

CRISPR-Cas9-generated deletion of *Ctr-ben-1* conferred resistance and caused a significant reduction in fitness (fecundity), which likely explains why just two high-impact variants were identified among wild strains and neither caused loss of *ben-1* function. Finally, because we hypothesized that similar selective pressures would cause the three *Caenorhabditis* species to evolve BZ resistance by mutation in a beta-tubulin gene, we assessed niche overlap among these species. *C.*

elegans occupies a niche distinct from *C. briggsae* and *C. tropicalis*, with only occasional overlap with *C. briggsae* [49, 50]. Consistent with this ecological separation, *ben-1* resistance alleles do not colocalize between species. The two *C. briggsae ben-1* resistance alleles were identified in strains collected in Aberdeen, Scotland (PE887) and Puerto Aventuras, Mexico (NIC1052), neither is a region where *C. elegans* has been sampled. *C. tropicalis* is found in warmer climates with no overlaps with *C. elegans* and rare overlaps with *C. briggsae*. Therefore, unique selection pressures potentially add to the independent evolution of BZ resistance driven by *ben-1* mutations. Overall, our results highlight the complexity of BZ resistance. Accurate prediction of BZ resistance across nematode species requires a clear understanding of the contributions of both beta-tubulin dependent and beta-tubulin independent mechanisms.

Nematode survival under BZ exposure depends on beta-tubulin dosage and drug-binding ability

BZs bind to beta-tubulins and inhibit the polymerization of microtubules [2–4]. Therefore, despite the presence of beta-tubulin independent resistance mechanisms [51,52], beta-tubulins have a large impact on BZ efficacy as an anthelmintic treatment. Two factors determine how beta-tubulin impacts susceptibility to BZs: (1) the beta-tubulin's ability to bind to BZs and (2) the dosage of the beta-tubulin protein, which can be modified by tissue-specific expression. Cell-specific expression of drug transporters or efflux pumps might also influence the intracellular BZ concentration. Nematode species have distinct beta-tubulin gene complements with divergence in number of genes, BZ binding affinities, expression levels and cell types, and redundancy. Ultimately, this divergence in beta-tubulin complement shapes the type(s) of resistance-associated alleles that arise in each nematode species. In species where the primary BZ-binding beta-tubulin is redundant with other isoforms, as in selfing *Caenorhabditis* species, loss of a single copy can confer resistance without disrupting essential microtubule functions. In species without redundancy, such as *H. contortus*, beta-tubulin variants that alter the BZ binding affinity are the only available beta-tubulin dependent route to BZ resistance.

In *C. elegans*, *ben-1* is the primary target of BZs but is redundant with *tbb-1* and *tbb-2* [28–30]. LoF alleles in *ben-1* reduce the total amount of BZ-binding protein while preserving essential microtubule functions, which permits nematode development during BZ exposure. A similar pattern likely occurs in *C. briggsae*, where rare high-impact variants in *ben-1* confer resistance, and other beta-tubulin genes maintain essential microtubule functions. Although natural *Ctr-ben-1* resistance alleles were not identified, a deletion of *ben-1* conferred BZ resistance in *C. tropicalis* but imposed a significant fitness cost, which could explain the few high-impact alleles among wild strains. Fewer *C. tropicalis* wild strains were surveyed (518) compared with *C. elegans* (611) and *C. briggsae* (641), which could partly explain why fewer high-impact variants were identified. Reduced variation in *Ctr-ben-1* might also partly reflect lower genome-wide *C. tropicalis* genetic diversity compared to *C. elegans* and *C. briggs*ae [53–55]. By contrast, *H. contortus* relies on the essential beta-tubulin *tbb-isotype-1* and cannot tolerate loss without severe fitness consequences [18]. The differences between the *Caenorhabditis* species and *H. contortus* demonstrate that the prediction of beta-tubulin dependent resistance requires the identification of the total number and expression levels of beta-tubulin genes and determination of which encoded beta-tubulins can bind to BZ. Altogether, BZ resistance depends not on the copy number of beta-tubulins alone but on the availability of functional beta-tubulins capable of interacting with BZs.

How can we accurately predict BZ resistance across nematode species?

To accurately predict BZ resistance across nematode species, we need (1) tractable nematode models with beta-tubulin gene complements that resemble that of parasite species, (2) improved parasitic nematode genomes that enable the comprehensive identification of beta-tubulin genes, (3) functional tests that define how parasite beta-tubulin alleles contribute to BZ response, and (4) to define the contribution of non-beta-tubulin genes to overall BZ response. To date, no experimentally tractable model nematode species exist with beta-tubulin genes that have both limited redundancy and BZ binding properties similar to those of parasitic nematodes. *Pristionchus pacificus*, a free-living clade V nematode has three beta-tubulin genes, comprising two *ben-1* orthologs (*Ppa-ben-1.1* and *Ppa-ben-1.2*) and an ortholog of *Cel-mec-7*

(*Ppa-mec-7*) [56]. All three beta-tubulin genes in *Pristionchus pacificus* are predicted to have high ABZ binding affinity (**S27 Fig**). Using CRISPR-Cas9 genome editing, we found that homozygous LoF alleles for either *Ppa-ben-1.1* or *Ppa-ben-1.2* could not be recovered in *P. pacificus*, suggesting that both genes are essential (**S13 Table**). The fact that *P. pacificus* has fewer beta-tubulin genes than *C. elegans* likely contributes to the lack of redundancy among beta-tubulins. The number, essentiality, and BZ binding affinity of the *P. pacificus* beta-tubulins more closely resembles that of *H. contortus*, which positions *P. pacificus* as a valuable free-living model to study essential beta-tubulin function, beta-tubulin dosage effects, and BZ resistance relevant to parasitic nematode species.

Second, to understand the role beta-tubulins play in BZ resistance across parasitic nematode species, we must significantly improve genomes and gene models. Most parasitic nematode genomes remain incomplete or are poorly annotated, which obscures beta-tubulin copy number and gene identity. Recent efforts have produced higher quality genomes for some parasitic nematodes [57–59], but we must still define beta-tubulin copy number across diverse nematode species. For example, improved reference genomes and gene models for *C. briggsae* [60,61] and *C. tropicalis* [53,55] enabled accurate beta-tubulin gene identification for these species. Until genome assemblies, technologies, and analytical techniques improve, we will be unable to accurately predict the number of beta-tubulin genes in a given species and their respective BZ binding affinities.

Third, functional validation of parasitic resistance alleles presents additional challenges. Although tools such as RNAi can work in parasitic nematodes [62], delivery challenges and difficulty isolating edited individuals limit its use. An alternative strategy is to introduce predicted parasite resistance alleles into *C. elegans* to test effects on fitness and BZ response, as shown previously [14–16]. Finally, some parasitic nematodes, such as ascarid species, exhibit BZ resistance without known beta-tubulin resistance alleles [63–65]. This pattern suggests that resistance arises independently of detected beta-tubulin sequence changes or reflects incomplete identification of beta-tubulin genes caused by poor genome assemblies. To date, the underlying cause of BZ resistance in ascarid species remains unclear. Reduced functional beta-tubulin dosage, altered BZ binding, or both could contribute to BZ resistance in ascarids [66]. Improved genome assemblies and annotation are required to identify all beta-tubulin genes and drug-binding sites to define the mechanisms of BZ resistance in ascarid species. In the future, the introduction of newly identified ascarid alleles into free-living nematode models can directly test resistance and fitness, and clarify the mechanisms that drive BZ resistance in clade III nematodes. Additionally, we must define how beta-tubulin redundancy, essentiality, dosage, and physical interactions with BZs shape the evolution of resistance to improve the prediction of BZ resistance across the huge diversity of parasitic nematode species.

Materials and methods

Identification of beta-tubulin loci

Amino acid sequences for all six *C. elegans* beta-tubulin proteins were obtained from WormBase (WS283) [67] and used as queries in a BLASTp search (Version 2.12.0) [68] against protein sequence databases constructed using gene models for *C. briggsae* [61] and *C. tropicalis* [53]. To construct the protein sequence database, we extracted gene model transcript features from the gene feature file with *gffread* (Version 0.9.11) [69] and processed them using the *makeblastdb* function from BLAST (Version 2.12.0). From the BLASTp search, we identified *C. briggsae* and *C. tropicalis* protein sequences with the highest percent identity (PID) to each *C. elegans* beta-tubulin protein. Only protein sequences with the highest PID in both searches were considered orthologs (**S14 Table**). For some *C. elegans* beta-tubulin orthologs, multiple *C. briggsae* or *C. tropicalis* gene models contained multiple splice isoforms. All gene models for all beta-tubulin transcripts were manually inspected, and isoforms that were not fully supported by short-read RNA sequencing data were removed.

Single nucleotide variant (SNV) and indel calling and annotation

To identify single nucleotide variants (SNVs) or indels (insertions and deletions) in the beta-tubulin genes across the selfing *Caenorhabditis* species, we used the Variant Annotation Tool from the *Caenorhabditis* Natural Diversity Resource (CaeNDR) (Release IDs: *C. elegans* - 20231213, *C. briggsae* - 20240129, *C. tropicalis* - 20231201) [35]. The identified

SNVs and indels included small insertions and deletions, frameshifts, altered stop and start codons, nonsynonymous changes, and splice variants (**S1**, **S2** **and** **S3 Tables**).

Structural variant (SV) calling and annotation

Structural variant (SV) calling was performed using *DELLY* (Version 0.8.3), a SV caller optimized to detect large insertions, deletions, and other complex structural variants such as inversions, translocations, and duplications in paired-end short-read alignments [70] and shown to perform well on *C. elegans* short-read sequence data [71]. SVs that overlapped with beta-tubulin genes were extracted using *bcftools* (Version 1.10.1) [72]. Insertions, deletions, inversions, and duplications that passed the *DELLY* (Version 0.8.3) default quality threshold (greater than three supporting read pairs with a median MAPQ > 20), filtered to high-quality genotypes (genotype quality > 15), and had at least one alternative allele were retained. For complex variants (inversions and duplications), the identification of at least one split-read pair was required (variants flagged as a precise SV by *DELLY*). To validate SVs that passed quality filtering, each SV was manually inspected for breakpoints in the raw-read alignments (*Wally*, Version 0.5.8) and for impacts on the beta-tubulin coding sequence (CaeNDR Genome Browser) [35] (**S15 Table**). We retained SVs where raw read alignments suggested that the SV impacted the beta-tubulin coding sequence. We compared the *Cel-ben-1* SVs called by *DELLY* to those SVs identified previously [71]. *DELLY* successfully recalled structural variants in several strains, including deletions in JU751, JU830, JU1395, JU2582, JU2587, JU2593, JU2829, and QX1233, as well as an inversion in MY518. However, *DELLY* did not detect a previously reported transposon insertion in strain JU3125. To assess if other SVs could have been missed by *DELLY*, we manually inspected the read alignments for all strains that had not been previously phenotyped to check if any other SVs were not detected by *DELLY*. We confirmed the presence of novel *Cel-ben-1* SVs in multiple strains, including putative deletions in ECA706 and NIC1832, and a duplication in NIC1107. Additionally, we identified a previously undetected putative deletion in JU4287. We also examined the amino acids at position 200 in TBB-1, TBB-2, MEC-7, TBB-4, and BEN-1 orthologs and found that all MEC-7, TBB-4, and BEN-1 orthologs contained phenylalanine, and that all TBB-1 and TBB-2 orthologs contained tyrosine at position 200 (**S27 Fig**).

Association of *Cel-ben-1* expression with ABZ response

Two previous assays measured developmental responses of wild *C. elegans* strains after ABZ exposure [14, 36]. For 180 of these wild *C. elegans* strains, whole-animal expression levels (transcripts per million estimates [TPM]) were collected from untreated young-adult animals [37]. We identified strains with low *Cel-ben-1* expression by selecting strains with TPM values more than one standard deviation (SD) below the mean expression level across all 207 wild strains with expression data. Of the 180 wild *C. elegans* strains, 105 strains were measured for both ABZ response and gene expression. A linear model was built using the *lm* function in R to account for assay effects. Subsequently, the residuals of the linear model were used to normalize previous measures of ABZ response. We evaluated the linear fit between each strain's expression of *ben-1* (**S1 Fig**), *tbb-1*, *tbb-2*, *mec-7*, or *tbb-4* (**S15 Fig**) and the developmental delay following ABZ exposure.

Phylogenetic analysis

We characterized the relatedness of isotype reference strains (genetically unique strains) with beta-tubulin variants using species trees downloaded from CaeNDR and generated by the 'post-gatk-nf' pipeline (https://github.com/AndersenLab/post-gatk-nf) (Release IDs: *C. elegans* - 20231213, *C. briggsae* - 20240129, *C. tropicalis* - 20231201) [35]. Briefly, the trees were generated using high-quality SNVs in isotype reference strains retained in the hard-filtered variant call format (VCF) file. *vcf2phylip* [73] and the *bioconvert* [74] function *phylip2stockholm* were used to prepare inputs for *quicktree*, which was used to construct a tree using a neighbor-joining algorithm [75]. All versions of these software can be accessed from the 'post-gatk' docker container (https://hub.docker.com/r/andersenlab/tree), used by the 'post-gatk-nf' pipeline. We visualized the trees for each species using the *ggtree* function from the *ggtree* (v3.6.2) R package [76].

Strain selection and maintenance

Eighteen *C. elegans* strains, 45 *C. briggsae* strains, and 15 *C. tropicalis* strains from the CaeNDR [35] were used in this study (S1, S2, **and S3 Table**). Isolation details for each strain are included in CaeNDR. For each species, we selected strains that had variants (SNV or SV) with unique high-impact consequences in *tbb-1*, *tbb-2*, *mec-7*, *tbb-4*, or *ben-1* that had not been previously phenotyped. High-impact consequences included changes to amino acids, start and stop codon positions, or splice variants predicted to disrupt beta-tubulin function [35]. Strains with high-impact consequences in a beta-tubulin gene are herein referred to as "predicted resistant" strains. Strains that were closely related to predicted resistant strains with no high-impact consequences in beta-tubulin genes were also included for *C. briggsae* and *C. tropicalis* and herein classified as "predicted susceptible" strains (S2, S3 Figs and **S4 Table**). Although these predicted susceptible strains are closely related to the predicted resistant strains, non-beta-tubulin variants in the genetic background of these strains could impact BZ susceptibility. The reference strains for all three species were included.

Before measuring ABZ responses, *C. elegans* and *C. briggsae* animals were maintained at 20ºC and *C. tropicalis* animals were maintained at 25ºC. All animals were maintained on 6 cm plates with modified nematode growth medium (NGMA), which contains 1% agar and 0.7% agarose to prevent animals from burrowing [77]. The NGMA plates were seeded with the *Escherichia coli* strain OP50 as a nematode food source. All strains were grown for three generations without starvation on NGMA plates before anthelmintic exposure to reduce the transgenerational effects of starvation stress [78].

CRISPR-Cas9 genome editing

To validate the role that *ben-1* plays in ABZ resistance in the three *Caenorhabditis* species, we used CRISPR-Cas9 to create *ben-1* deletions. For *C. elegans*, we used a previously generated strain (ECA882) with a *ben-1* deletion in the N2 background [14,15,32,36]. The *ben-1* deletions were generated in the AF16 background for *C. briggsae* and the NIC58 background for *C. tropicalis*. Injections were performed by InVivo Biosystems (Eugene, OR), and deletions of *Cbr-ben-1* and *Ctr-ben-1* were confirmed using PCR (**S10 and S11 Figs**). Briefly, two primer pairs were designed for the deletion alleles for each species, with each pair designed to bind to a region external or internal to both of the deletions. Confirmation of deletion was performed by performing two amplification reactions for each sample: (1) the use of both external primers, and (2) the use of an internal and external pair (**S5 Table**). The parental strain was used as a control in each PCR. Deletions were confirmed by a reduction in the size of the external-external amplicon in the edited strains compared to the unedited parental control strain. Homozygosity was confirmed by the loss of a band amplified from the external-internal primer pair. Edited strains underwent two generations of PCR confirmation for homozygosity. Two independent edits of each allele in each species were generated to control for any potential off-target effects caused by CRISPR-Cas9 genome editing (**S12**, **S13 Figs and S5 Table**).

Nematode food preparation for NGMA 6 cm plates

The OP50 *E. coli* strain was used as a nematode food source for NGMA plates. A frozen stock of OP50 was streaked onto a 10 cm Luria-Bertani (LB) agar plate and incubated overnight at 37ºC. The following day, a single bacterial colony was transferred into each of two culture tubes that contained 5 mL of 1x LB. The starter cultures and two negative controls (1X LB without *E. coli*) were incubated for 18 hours at 37ºC shaking at 210 rpm. The OD_{600} value of the starter cultures were measured using a spectrophotometer (BioRad, SmartSpec Plus) to calculate how much starter culture was needed to inoculate a 1 L culture at an OD_{600} value of 0.005. For each assay, one culture containing 1 L of pre-warmed 1X LB inoculated with the starter culture grew for approximately 4 - 4.5 hours at 37ºC at 210 rpm to an OD_{600} value between 0.45 and 0.6. Cultures were transferred to 4ºC to slow growth. OP50 was spotted on NGMA test plates (two per culture) and grown at 37ºC overnight to assay for contamination.

Nematode food preparation for high-throughput larval development assays (HTLDAs)

One batch of HB101 *E. coli* was used as a nematode food source for all HTLDAs in this study. A frozen stock of HB101 *E. coli* was streaked onto a 10 cm LB agar plate and incubated overnight at 37ºC. The following day, a single bacterial colony was transferred into three culture tubes that contained 5 mL of 1x Horvitz Super Broth (HSB). The starter cultures and two negative controls (1X HSB without *E. coli*) were incubated for 18 hours at 37ºC shaking at 180 rpm. The OD_{600} value of the starter cultures were measured using a spectrophotometer (BioRad, SmartSpec Plus) to calculate how much starter culture was needed to inoculate a 1 L culture at an OD_{600} value of 0.001. A total of four cultures each containing 1 L of pre-warmed 1X HSB inoculated with the starter culture grew for 15 hours at 37ºC while shaking at 180 rpm. After 15 hours, flasks were removed from the incubator and transferred to 4ºC to slow growth. The 1X HSB was removed from the cultures by performing three rounds of centrifugation, where the supernatant was removed, and the bacterial cells were pelleted. Bacterial cells were washed with K medium, resuspended in K medium, pooled, and transferred to a 2 L glass beaker. The OD_{600} value of the bacterial suspension was measured and diluted to a final concentration of OD_{600}100 with K medium, aliquoted to 15 mL conical tubes, and stored at -80ºC for use in the HTLDAs.

ABZ dose-response assays for *C. briggsae* and *C. tropicalis*

Because ABZ response had been minimally characterized in *C. briggsae* [79] and has not yet been described in *C. tropicalis*, we first measured dose-response curves for both species after exposure to ABZ to assess developmental delay. Before performing HTLDAs, ABZ (Sigma-Aldrich, Catalog # A4673-10G) stock solutions were prepared in dimethyl sulfoxide (DMSO) (Fisher Scientific, Catalog # D1281), aliquoted, and stored at -20ºC for use in the assays. For the dose-response assays, animals were exposed to ABZ at the following concentrations (μM): 0 (0.3% DMSO), 0.12, 0.23, 0.47, 0.94, 1.88, 3.75, 7.5, 15, 30, 60, and 120. Animals developed in the presence of ABZ as described in *HTLDAs to assess nematode development*.

Dose-response model estimation and statistics were performed as described previously [80,81]. Briefly, a four-parameter log-logistic dose-response curve was fit independently for a genetically diverse set of 11 *C. briggsae* strains (**Fig 3**) and seven *C. tropicalis* strains (**Fig 6**), where normalized median animal length was used as a metric for phenotypic response (see *HTLDA data collection and data cleaning*). For each strain-specific dose-response model, slope (*b*) and concentration (*e*) were estimated with strain as a covariate. We calculated EC_{10} as we have previously found EC_{10} response to be more heritable than half maximal effective concentration (EC_{50}) estimates and were used in our analysis [80,81]. A dosage of 30 μM ABZ was closest to the EC_{10} for *C. briggsae* and *C. tropicalis*, consistent with ABZ concentrations used in past *C. elegans* assays [15,16,36] and in all HTLDAs in this study.

HTLDAs to assess nematode development

Populations of each strain were amplified and bleach-synchronized in three independent assays. Independent bleach synchronizations controlled for variation in embryo survival and subsequent effects on developmental rates. After bleach synchronization, approximately 30 embryos were dispensed into each well of a 96-well microplate in 50 μL of K medium. Each strain had sixteen wells per condition (DMSO or ABZ) in each assay. Three independent assays yielded a total of forty-eight wells per condition per strain. Each 96-well microplate was prepared, labeled, and sealed using gas-permeable sealing films (Fisher Scientific, Catalog # 14-222-043). Plates were placed in humidity chambers to incubate for 24 hours at 20°C for *C. elegans* and *C. briggsae*, and 25°C for *C. tropicalis* while shaking at 170 rpm (INFORS HT Multitron shaker). After 24 hours, every plate was inspected to ensure that all embryos hatched and animals were developmentally arrested at the first larval (L1) stage so all strains started each assay at the same developmental stage. Next, food was prepared to feed the developmentally arrested L1 animals using the required number of OD_{600}100 HB101 aliquots (see *Nematode food preparation for HTLDAs*). The HB101 aliquots were thawed at room temperature, combined

into a single conical tube, and diluted to an OD_{600}30 with K medium. To inhibit further bacterial growth and prevent contamination, 150 μL of kanamycin was added to the HB101. An aliquot of 100 μM ABZ stock solution was thawed at room temperature and added to an aliquot of OD_{600}30 K medium at a 3% volume/volume ratio. Next, 25 μL of the food and ABZ mixture was transferred into the appropriate wells of the 96-well microplates to feed the arrested L1 animals at a final HB101 concentration of OD_{600}10 and expose L1 animals to ABZ. Immediately afterward, the 96-well microplates were sealed using a new gas permeable sealing film, returned to the humidity chambers, and incubated for 48 hours at 20°C (*C. elegans* and *C. briggsae*) or 42 hours at 25°C (*C. tropicalis*) while shaking at 170 rpm. After 48 hours (*C. elegans* and *C. briggsae*) or 42 hours (*C. tropicalis*) of incubation and shaking in the presence of food and either 0.3% DMSO or 30 μM ABZ, the 96-well microplates were removed from the incubator and treated with 50 mM sodium azide in M9 for 10 minutes to paralyze and straighten nematodes. After 10 minutes, images of nematodes in the microplates were immediately captured using the Molecular Devices ImageXpress Nano microscope (Molecular Devices, San Jose, CA) using a 2X objective. The ImageXpress Nano microscope acquires brightfield images using a 4.7 megapixel CMOS camera and stores images in a 16-bit TIFF format. The images were used to quantify the development of nematodes in the presence of DMSO or ABZ as described below (see *HTLDA data collection and data cleaning*). A full step-by-step protocol for the HTLDA has been deposited on protocols.io [82].

HTLDA data collection and data cleaning

CellProfiler (Version 24.10.1) was used to characterize and quantify biological data from the image-based assays. Custom software packages designed to extract animal measurements from images collected on the Molecular Devices ImageXpress Nano microscope were previously described [39]. *CellProfiler* modules and *WormToolbox* were developed to extract morphological features of individual animals from images from the HTLDA [82]. Worm model estimations and custom *CellProfiler* pipelines were written using the *WormToolbox* in the GUI-based instance of *CellProfiler* [39]. Next, a Nextflow pipeline (Version 24) was written to run command-line instances of *CellProfiler* in parallel on the Rockfish High-Performance Computing Cluster (Johns Hopkins University). The *CellProfiler* workflow can be found at https://github.com/AndersenLab/cellprofiler-nf. The custom *CellProfiler* pipeline generates animal measurements by using four worm models: three worm models tailored to capture animals at the L4 larval stage, in the L2 and L3 larval stages, and the L1 larval stage, as well as a "multi-drug high dose" (MDHD) model, to capture animals with more abnormal body sizes caused by extreme anthelmintic responses. These measurements comprised our raw dataset. Two *C. briggsae* strains (NIC1052 and VX34) were not fully paralyzed and straightened at the time of imaging, which created some misclassification of animal measurements. Thus, the animal lengths for strains NIC1052 and VX34 measured by *CellProfiler* are shorter than the actual animal lengths. However, the difference in animal lengths does not affect the classification of a strain as resistant or sensitive to ABZ. Data cleaning and analysis steps were performed using a custom R package, *easyXpress* (Version 2.0) [39] and followed methods previously reported [36]. Briefly, using *easyXpress*, we removed statistical outlier measurements for each strain by condition to reduce the likelihood that statistical outliers influence anthelmintic responses. Finally, we normalized the data by (1) regressing variation attributable to assay and technical replicate effects and (2) normalizing these extracted residual values to the average control phenotype. These normalized length measurements (*i.e.*, normalized animal length (μm)) have the helpful property of being centered on zero in control conditions for each strain, and therefore, control for the differences in the average lengths of the strains. All analyses were performed using the R statistical environment (Version 4.2.1) unless stated otherwise.

C. briggsae and *C. tropicalis* fecundity assays

To define the fitness costs associated with a loss of *ben-1* in *C. briggsae* and *C. tropicalis*, we performed fecundity assays. For *C. briggsae*, we used the two strains with independent edits of *ben-1* in the AF16 background (ECA3953 and ECA3954) and the AF16 reference strain. For *C. tropicalis*, we used the two strains with independent edits of *ben-1* in the

NIC58 background (ECA4247 and ECA4248) and the NIC58 reference strain. To perform fecundity assays, we placed a single L4 larval stage hermaphrodite from each strain onto a 6 cm NGMA plate that was spotted with *E. coli* OP50. *C. briggsae* assay plates were maintained at 20°C, and *C. tropicalis* assay plates were maintained at 25°C. For each assay plate, the original hermaphrodite parent was transferred to a fresh 6 cm NGMA plate every 24 hours for 192 hours. Ten technical replicates were prepared for each strain. The Basic Imaging Platform from Tau Scientific was used to collect images for each of the assay plates (0, 24, 48, 72, 96, and 120-hours) at either 48 or 72 hours for *C. briggsae* and *C. tropicalis* animals, respectively, after the removal of the parent from each NGMA plate. The total offspring was counted from each image by visual inspection using the Multi-point tool in ImageJ (Version 1.54g). The original hermaphrodite parents were excluded from the counts. Replicates where the original hermaphrodite parent died were excluded from the analysis. Only biological replicates with data from at least six assay plates were used to calculate total fecundity (**Fig 4**, **S6** **and** **S7 Tables**).

Tissue-specific beta-tubulin gene expression conservation in *C. elegans*, *C. briggsae*, and *C. tropicalis*

To assess beta-tubulin expression divergence across neuronal cell classes, we used whole-animal single-cell transcriptomes of *C. elegans*, *C. briggsae*, and *C. tropicalis* [43]. We quantified neuronal cell expression divergence across species using precomputed Jaccard distances calculated from the neuronal cell classes in at least one species and the number of neuron classes in which a gene is expressed in all three species [43]. We also downloaded gene expression summary data for each homologous cell class from *CaenoGen* and analyzed expression patterns in cell classes that used acetylcholine (ACh) as a neurotransmitter in *C. elegans* [83]. We identified cell classes in which *ben-1* orthologs showed species-specific presence or absence of expression.

We also analyzed embryonic single-cell transcriptomes from the *C. briggsae* and *C. elegans* reference strains to examine the conservation of beta-tubulin gene expression in homologous cell types [44]. We used pre-computed summary statistics to quantify two components of expression divergence among beta-tubulin genes: gene distance (reported as Jensen-Shannon Distances for each gene) and expression breadth (reported as Tau metrics for each species). Beta-tubulin gene distances and expression breadth metrics are available in the gene data summary table file (S9 and S10 Tables). Estimates for three cell populations are distinguished by cell-type assignment: progenitor, terminal, and joint (combined progenitor and terminal cells).

Protein structure and visualization of *ben-1* and *tbb-isotype-1* variants

For *C. elegans*, the BEN-1 amino acid sequence was obtained from WormBase (WS283) [67]. For *C. briggsae* and *C. tropicalis*, BEN-1 amino acid sequences were the best hits to the *C. elegans* BEN-1 query from the reciprocal BLASTp search used to identify beta-tubulin orthologs (*see Identification of beta-tubulin loci*) (**S16 Table**). The *H. contortus tbb-isotype-1* amino acid sequence was obtained from WormBase Parasite (Version: WBPS19) [42]. Protein structures were predicted using AlphaFold3 [84]. All BEN-1 variant data and associated benzimidazole-response phenotypes were compiled from this study and previously published data [14,36]. A custom Python script was used to generate a PyMOL script (Version 3.1.6.1) for structural visualization. Each predicted beta-tubulin structure was aligned to *Cel*-BEN-1 using the PyMOL `*align*` command.

Mutation of *ben-1* orthologs in *Pristionchus pacificus*

To test the function of *ben-1* in *Pristionchus pacificus*, we used CRISPR-Cas9 genome editing to delete the two orthologs of *Cel-ben-1*. Designed crRNAs and tracrRNA were synthesized by Integrated DNA Technologies (IDT). For the creation of the guide RNAs, 3 µL of 100 µM tracrRNA (IDT) was combined with 3 µL of 100 µM crRNA (IDT) and incubated at 95ºC for five minutes, followed by five minutes at room temperature for annealing. The ribonucleoprotein (RNP) complex was then created by combining 0.61 µL of the guide-RNA mixture with 0.25 µL of Cas9 protein (IDT), followed by incubation at

37ºC for 10 minutes. The final microinjection mix was then created by combining the 0.86 μL RNP complex with 9.14 μL of a TE buffer mixture containing a (55 ng/μL) plasmid containing a *P. pacificus* codon-optimized *egl-20p::TurboRFP::rpl-23UTR* construct [85] used as a co-injection marker for visual identification of successful injections by the presence of fluorescent F1 individuals (**S13 Table**). All F1 individuals displaying fluorescence were then isolated and allowed to self-fertilize. After successful F2 embryo hatching, F1 individuals were genotyped for mutations using a heteroduplex mobility assay (HMA). Individuals from F2 broods that were determined to contain heterozygous mutations in F1 mothers were then isolated, allowed to self-fertilize, and genotyped by HMA after F3 embryos had hatched to identify homozygous mutant lines, followed by Sanger sequencing to determine types of mutations induced. Additionally, for mutations that were homozygous lethal, the F3 from heterozygous F2 individuals were likewise genotyped by HMA to quantify survivability based on deviations from expected Mendelian ratios.

Supporting information

S1 Fig. The relationship between *ben-1* expression levels and albendazole response in *C. elegans* strains. (A) Scatterplot of the relationship between *ben-1* expression levels and normalized albendazole (ABZ) response across *C. elegans* wild strains. Each point represents a strain phenotyped for ABZ response in previous publications [14, 36] with *ben-1* expression data [37]. The *ben-1* expression level measured in transcripts per million (TPM) is displayed on the x-axis. The normalized ABZ response values adjusted for assay-specific effects are displayed on the y-axis. The gray line represents the linear regression fit between *ben-1* expression and normalized response ($R^2 = 0.34$, p-value = 5.16e-18), with the linear model's coefficient of determination (R^2). Data points are colored based on the predicted functional consequence of the *ben-1* allele for each strain (*i.e.*, large structural variant (SV), frameshift, missense substitution, disrupted start/stop sequence, no high-impact variant, or low *ben-1* expression). (B) Boxplots of *ben-1* expression levels among strains grouped by the predicted functional consequences of their *ben-1* alleles. Each point represents the *ben-1* expression level of an individual within each group. We tested for statistically significant differences in the expression between each consequence type and wild strains without a high-impact *ben-1* allele with an unpaired Wilcoxon test. Significance levels are indicated by symbols: '*' ($p < 0.05$), '**' ($p < 0.01$), '***' ($p < 0.001$), '****' ($p < 0.0001$).
(TIFF)

S2 Fig. *C. briggsae* species tree highlighting isotype reference strains tested for ABZ resistance. *C. briggsae* strains included in high-throughput larval development assays (HTLDAs) are highlighted on the *C. briggsae* species tree. Strains with predicted high-impact variants in a beta-tubulin gene are denoted by red points. Strains with no predicted variants in any beta-tubulin gene are denoted by gray points.
(TIFF)

S3 Fig. *C. tropicalis* species tree highlighting isotype reference strains tested for ABZ resistance. *C. tropicalis* strains included in high-throughput larval development assays (HTLDAs) are highlighted on the *C. tropicalis* species tree. Strains with predicted high-impact variants in a beta-tubulin gene are denoted by red points. Strains with no predicted variants in any beta-tubulin gene are denoted by gray points.
(TIFF)

S4 Fig. HTLDAs for *C. elegans* strains with high-impact BEN-1 variants in control conditions. Median animal length values from populations of nematodes grown in DMSO are shown on the y-axis. Each point represents the median animal length from a well containing approximately five to 30 animals. Data are shown as Tukey box plots with the median as a solid horizontal line, the top and bottom of the box representing the 75th and 25th quartiles, respectively. The top whisker is extended to the maximum point that is within a 1.5 interquartile range from the 75th quartile. The bottom whisker is extended to the minimum point that is within the 1.5 interquartile range from the 25th quartile. Results for (A) the N2

reference strain (orange) and a strain with a *ben-1* deletion in the N2 background (red), and (B) all wild *C. elegans* strains with unique high-impact variants in *ben-1* are sorted by their relative resistance to ABZ based on median animal length. Wild *C. elegans* strains are colored by beta-tubulin variant status.
(TIF)

S5 Fig. HTLDAs for *C. briggsae* strains with high-impact BEN-1 variants in control conditions. Median animal length values from populations of nematodes grown in DMSO are shown on the y-axis. Each point represents the median animal length from a well containing approximately five to 30 animals. Data are shown as Tukey box plots with the median as a solid horizontal line, the top and bottom of the box representing the 75th and 25th quartiles, respectively. The top whisker is extended to the maximum point that is within a 1.5 interquartile range from the 75th quartile. The bottom whisker is extended to the minimum point that is within the 1.5 interquartile range from the 25th quartile. Results for (A) the AF16 reference strain (green) and two strains each with an independent *ben-1* deletion in the AF16 background (ECA3953 and ECA3954) (red), and (B) all wild *C. briggsae* strains with unique high-impact variants in *ben-1* are sorted by their relative resistance to ABZ based on median animal length. No variant (N. V.) strains (gray) paired with strains that have a high-impact variant in a beta-tubulin gene are shown alongside each corresponding strain with a high-impact variant in a beta-tubulin gene. Wild *C. briggsae* strains are colored by beta-tubulin variant status.
(TIF)

S6 Fig. HTLDAs for *C. tropicalis* strains with high-impact TBB-2 or BEN-1 variants with paired predicted susceptible strains in control conditions. Median animal length values from populations of nematodes grown in DMSO are shown on the y-axis. Each point represents the median animal length from a well containing approximately five to 30 animals. Data are shown as Tukey box plots with the median as a solid horizontal line, the top and bottom of the box representing the 75th and 25th quartiles, respectively. The top whisker is extended to the maximum point that is within a 1.5 interquartile range from the 75th quartile. The bottom whisker is extended to the minimum point that is within the 1.5 interquartile range from the 25th quartile. Results for (A) the NIC58 reference strain (blue) and two strains each with an independent *ben-1* deletion in the NIC58 background (ECA4247 and ECA4248) (red), and (B) all wild *C. tropicalis* strains with unique high-impact variants in *ben-1* or *tbb-2* are sorted by their relative resistance to ABZ based on median animal length. No variant (N. V.) strains (gray) paired with strains that have a high-impact variant in a beta-tubulin gene are shown alongside each corresponding strain with a high-impact variant in a beta-tubulin gene. Wild *C. tropicalis* strains are colored by beta-tubulin variant status.
(TIF)

S7 Fig. HTLDAs for each *C. elegans* strain with a high-impact variant in BEN-1 in albendazole. The regressed median animal length values for populations of nematodes grown in 30 μM albendazole (ABZ) are shown on the y-axis. Each point represents the normalized median animal length value of a well containing approximately five to 30 animals. Data are shown as Tukey box plots with the median as a solid horizontal line, and the top and bottom of the box representing the 75th and 25th quartiles, respectively. The top whisker is extended to the maximum point that is within the 1.5 interquartile range from the 75th quartile. The bottom whisker is extended to the minimum point that is within the 1.5 interquartile range from the 25th quartile. The gray dashed line marks the *C. elegans* resistance threshold, defined as two standard deviations below the mean of the *ben-1* deletion strain in the N2 reference strain background. Results for the N2 reference strain (orange) and all wild *C. elegans* strains with unique high-impact variants in *ben-1* are sorted by their relative resistance to ABZ based on median animal length. Wild *C. elegans* strains are colored by beta-tubulin variant status.
(TIF)

S8 Fig. HTLDAs *C. briggsae* strains with a high-impact variant in BEN-1 with paired predicted susceptible strains in albendazole. The regressed median animal length values for populations of nematodes grown in 30 μM albendazole

(ABZ) are shown on the y-axis. Each point represents the normalized median animal length value of a well containing approximately five to 30 animals. Strains are sorted by their relative resistance to ABZ based on median animal length. Data are shown as Tukey box plots with the median as a solid horizontal line, and the top and bottom of the box representing the 75th and 25th quartiles, respectively. The top whisker is extended to the maximum point that is within the 1.5 interquartile range from the 75th quartile. The bottom whisker is extended to the minimum point that is within the 1.5 interquartile range from the 25th quartile. The gray dashed line marks the *C. briggsae* resistance threshold, defined as two standard deviations below the mean of the *ben-1* deletion strain in the AF16 reference strain background. No variant (N. V.) strains (gray) paired with strains that have a high-impact variant in the *ben-1* gene are shown alongside each corresponding strain with a high-impact variant in *ben-1*. Wild *C. briggsae* strains are colored by beta-tubulin variant status.
(TIF)

S9 Fig. HTLDAs for *C. tropicalis* strains with high-impact variants in TBB-2 or BEN-1 with paired predicted susceptible strains in albendazole. The regressed median animal length values for populations of nematodes grown in 30 μM albendazole (ABZ) are shown on the y-axis. Each point represents the normalized median animal length value of a well containing approximately five to 30 animals. Data are shown as Tukey box plots with the median as a solid horizontal line, and the top and bottom of the box representing the 75th and 25th quartiles, respectively. The top whisker is extended to the maximum point that is within the 1.5 interquartile range from the 75th quartile. The bottom whisker is extended to the minimum point that is within the 1.5 interquartile range from the 25th quartile. The gray dashed line marks the *C. tropicalis* resistance threshold, defined as two standard deviations below the mean of the *ben-1* deletion strain in the NIC58 reference strain background. No variant (N. V.) strains (gray) paired with strains that have a high-impact variant in the *tbb-2* or *ben-1* genes are shown alongside each corresponding strain with a high-impact variant in *tbb-2* or *ben-1*. Wild *C. tropicalis* strains are colored by beta-tubulin variant status.
(TIF)

S10 Fig. PCR confirmation of the *ben-1* deletion in the *C. briggsae* reference strain background, AF16. Three primer pairs were used to confirm the deletion of *ben-1* in the *C. briggsae* reference strain, AF16. The oECA2728 (external) and oECA2803 (internal) primers flank either side of the guide region on the 5' end. The oECA2730 (internal) and oECA2731 (external) primers flank either side of the guide region on the 3' end. The oECA2728 and oECA2731 primers flank the outside of the *ben-1* region to be deleted. The wild-type (AF16) region spans 1383 base pairs (bp), while the *ben-1* deletion is reduced to 732 bp. The top of the gel is labeled by the three strains: PB420 (AF16) and the two independently edited *ben-1* deletion strains in the AF16 background (ECA3953 and ECA3954). Each well of the gel is labeled by the primer pair used. The Invitrogen 1 Kb Plus DNA Ladder is shown on each side of the gel.
(TIFF)

S11 Fig. PCR confirmation of the *ben-1* deletion in the *C. tropicalis* reference strain background, NIC58. Three primer pairs were used to confirm the deletion of *ben-1* in the *C. tropicalis* reference strain background, NIC58. The oECA2734 (internal) and oECA2735 (external) primers flank either side of the guide region on the 3' end. The oECA2732 and oECA2735 primers flank the *ben-1* region to be deleted. The wild-type (NIC58) region spans 1538 base pairs (bp), and the *ben-1* deletion reduces the region to 513 bp. The top of the gel is labeled by the three strains: NIC58 and the two independently edited *ben-1* deletion strains in the NIC58 background (ECA4247 and ECA4248). Each well of the gel is labeled by the primer pair used. The Invitrogen 1 Kb Plus DNA Ladder is shown on each side of the gel.
(TIFF)

S12 Fig. High-throughput larval development assays for two independently edited *C. briggsase* AF16 strains with a loss of *ben-1*. The regressed median animal length values for populations of nematodes grown in 30 μM albendazole (ABZ) are shown on the y-axis. Each point represents the normalized median animal length value of a well containing

approximately five to 30 animals. Data are shown as Tukey box plots with the median as a solid horizontal line, and the top and bottom of the box representing the 75th and 25th quartiles, respectively. The top whisker is extended to the maximum point that is within the 1.5 interquartile range from the 75th quartile. The bottom whisker is extended to the minimum point that is within the 1.5 interquartile range from the 25th quartile. The gray dashed line marks the *C. briggsae* resistance threshold, defined as two standard deviations below the mean of the *ben-1* deletion strain (ECA3953) in the AF16 reference strain background. Results are shown for the AF16 reference strain (green) and two independently edited strains with a *ben-1* deletion in the AF16 background (ECA3953 and ECA3954) (red).
(TIFF)

S13 Fig. High-throughput larval development assays for two independently edited *C. tropicalis* NIC58 strains with a loss of *ben-1*. The regressed median animal length values for populations of nematodes grown in 30 μM albendazole (ABZ) are shown on the y-axis. Each point represents the normalized median animal length value of a well containing approximately five to 30 animals. Data are shown as Tukey box plots with the median as a solid horizontal line, and the top and bottom of the box representing the 75th and 25th quartiles, respectively. The top whisker is extended to the maximum point that is within the 1.5 interquartile range from the 75th quartile. The bottom whisker is extended to the minimum point that is within the 1.5 interquartile range from the 25th quartile. The gray dashed line marks the *C. tropicalis* resistance threshold, defined as two standard deviations below the mean of the *ben-1* deletion strain (ECA24248) in the NIC58 reference strain background. Results are shown for the NIC58 reference strain (blue) and two independently edited strains with a *ben-1* deletion in the NIC58 background (ECA4247 and ECA4248) (red).
(TIFF)

S14 Fig. Relationship between missense substitutions in BEN-1 and albendazole response in *C. elegans* strains. Scatterplots show the relationship between normalized median animal length (y-axis) and three amino acid substitution scoring metrics (x-axis): BLOSUM62 ($R^2 = 0.97$, p-value = 0.11), Grantham ($R^2 = 0.39$, p-value = 0.57), and percent protein ($R^2 = 0.1$, p-value = 0.8). Each point represents a *C. elegans* strain with a missense substitution in BEN-1. Gray lines indicate the linear regression fit for these models. (A) Strains phenotyped for ABZ response in previous assays are plotted [14, 36]. (B) Strains phenotyped in the assays performed for this study are plotted.
(TIFF)

S15 Fig. The relationship between *C. elegans* beta-tubulin expression and albendazole response. Scatterplot of the relationship between (A) *tbb-1*, (B) *tbb-2*, (C) *mec-7*, and (D) *tbb-4* expression levels and normalized albendazole (ABZ) response across *C. elegans* wild strains. Each point represents a strain phenotyped for ABZ response in previous publications (Hahnel *et al.*, 2018; Shaver *et al.*, 2024) with *tbb-1, tbb-2*, *mec-7*, and *tbb-4* expression data [37]. The *tbb-1*, *tbb-2*, *mec-7*, and *tbb-4* expression levels measured in transcripts per million (TPM) are displayed on the x-axis. The normalized ABZ response values adjusted for assay-specific effects are displayed on the y-axis. The gray line represents the linear regression fit between beta-tubulin gene expression and normalized response, with the linear model's coefficient of determination (R^2). Data points are colored based on the predicted functional consequence of their *ben-1* alleles (*i.e.*, large structural variant (SV), frameshift, missense substitution, disrupted start/stop sequence, no high-impact variant, or low *ben-1* expression).
(TIFF)

S16 Fig. High-throughput larval development assays for each *C. elegans* strain with a high-impact variant in MEC-7 or TBB-4 with paired predicted susceptible strains in control conditions. Median animal length values from populations of nematodes grown in DMSO are shown on the y-axis. Each point represents the median animal length from a well containing approximately five to 30 animals. Data are shown as Tukey box plots with the median as a solid horizontal line, the top and bottom of the box representing the 75th and 25th quartiles, respectively. The top whisker is extended

to the maximum point that is within a 1.5 interquartile range from the 75th quartile. The bottom whisker is extended to the minimum point that is within the 1.5 interquartile range from the 25th quartile. No variant (N. V.) strains (gray) paired with strains that have a high-impact variant in a beta-tubulin gene are shown alongside each corresponding strain with a high-impact variant in a beta-tubulin gene. Wild *C. elegans* strains are colored by beta-tubulin variant status.
(TIF)

S17 Fig. High-throughput larval development assays for each *C. briggsae* strain with a high-impact variant in TBB-1, TBB-2, MEC-7, or TBB-4 with paired predicted susceptible strains in control conditions. Median animal length values from populations of nematodes grown in DMSO are shown on the y-axis. Each point represents the median animal length from a well containing approximately five to 30 animals. Data are shown as Tukey box plots with the median as a solid horizontal line, the top and bottom of the box representing the 75th and 25th quartiles, respectively. The top whisker is extended to the maximum point that is within a 1.5 interquartile range from the 75th quartile. The bottom whisker is extended to the minimum point that is within the 1.5 interquartile range from the 25th quartile. No variant (N. V.) strains (gray) paired with strains that have a high-impact variant in a beta-tubulin gene are shown alongside each corresponding strain with a high-impact variant in a beta-tubulin gene. Wild *C. briggsae* strains are colored by beta-tubulin variant status.
(TIF)

S18 Fig. High-throughput larval development assays for each *C. tropicalis* strain with a high-impact variant in MEC-7 or TBB-4 with paired predicted susceptible strains in control conditions. Median animal length values from populations of nematodes grown in DMSO are shown on the y-axis. Each point represents the median animal length from a well containing approximately five to 30 animals. Data are shown as Tukey box plots with the median as a solid horizontal line, the top and bottom of the box representing the 75th and 25th quartiles, respectively. The top whisker is extended to the maximum point that is within a 1.5 interquartile range from the 75th quartile. The bottom whisker is extended to the minimum point that is within the 1.5 interquartile range from the 25th quartile. No variant (N. V.) strains (gray) paired with strains that have a high-impact variant in a beta-tubulin gene are shown alongside each corresponding strain with a high-impact variant in a beta-tubulin gene. Wild *C. tropicalis* strains are colored by beta-tubulin variant status.
(TIF)

S19 Fig. High-throughput larval development assays for each *C. elegans* strain with a high-impact variant in MEC-7 or TBB-4 in the presence of albendazole. The regressed median animal length values for populations of nematodes grown in 30 μM albendazole (ABZ) are shown on the y-axis. Each point represents the normalized median animal length value of a well containing approximately five to 30 animals. Data are shown as Tukey box plots with the median as a solid horizontal line, and the top and bottom of the box representing the 75th and 25th quartiles, respectively. The top whisker is extended to the maximum point that is within the 1.5 interquartile range from the 75th quartile. The gray dashed line marks the *C. elegans* resistance threshold, defined as two standard deviations below the mean of the *ben-1* deletion strain in the N2 reference strain background. The bottom whisker is extended to the minimum point that is within the 1.5 interquartile range from the 25th quartile. No variant (N. V.) strains (gray) paired with strains that have a high-impact variant in a beta-tubulin gene are shown alongside each corresponding strain with a high-impact variant in a beta-tubulin gene. Wild *C. elegans* strains are colored by beta-tubulin variant status.
(TIF)

S20 Fig. High-throughput larval development assays for each *C. briggsae* strain with a high-impact variant in TBB-2, MEC-7, or TBB-4 in the presence of albendazole. The regressed median animal length values for populations of nematodes grown in 30 μM albendazole (ABZ) are shown on the y-axis. Each point represents the normalized median animal length value of a well containing approximately five to 30 animals. Data are shown as Tukey box plots with the median

as a solid horizontal line, and the top and bottom of the box representing the 75th and 25th quartiles, respectively. The top whisker is extended to the maximum point that is within the 1.5 interquartile range from the 75th quartile. The bottom whisker is extended to the minimum point that is within the 1.5 interquartile range from the 25th quartile. The gray dashed line marks the *C. briggsae* resistance threshold, defined as two standard deviations below the mean of the *ben-1* deletion strain in the AF16 reference strain background. Results for the AF16 reference strain and all *C. briggsae* wild strains with unique high-impact variants in (A) TBB-1 and TBB-2 and (B) TBB-4 and MEC-7 are shown. No variant (N. V.) strains (gray) paired with strains that have a high-impact variant in a beta-tubulin gene are shown alongside each corresponding strain with a high-impact variant in a beta-tubulin gene. Wild *C. tropicalis* strains are colored by beta-tubulin variant status.
(TIF)

S21 Fig. High-throughput larval development assays for each *C. tropicalis* strain with a high-impact variant in MEC-7 or TBB-4, and paired predicted susceptible strains in the presence of albendazole. The regressed median animal length values for populations of nematodes grown in 30 μM albendazole (ABZ) are shown on the y-axis. Each point represents the normalized median animal length value of a well containing approximately five to 30 animals. Data are shown as Tukey box plots with the median as a solid horizontal line, and the top and bottom of the box representing the 75th and 25th quartiles, respectively. The top whisker is extended to the maximum point that is within the 1.5 interquartile range from the 75th quartile. The bottom whisker is extended to the minimum point that is within the 1.5 interquartile range from the 25th quartile. The gray dashed line marks the *C. tropicalis* resistance threshold, defined as two standard deviations below the mean of the *ben-1* deletion strain in the NIC58 reference strain background. No variant (N. V.) strains (gray) paired with strains that have a high-impact variant in a beta-tubulin gene are shown alongside each corresponding strain with a high-impact variant in a beta-tubulin gene. Wild *C. tropicalis* strains are colored by beta-tubulin variant status.
(TIF)

S22 Fig. The global distribution of *Caenorhabditis* strains with predicted high-impact variation in *tbb-1*. Each point represents an isotype reference strain with a predicted high-impact variant in *tbb-1*. (A) Each point corresponds to the sampling location of the strain. (B) Each point corresponds to the location of the strain in a genome-wide phylogeny of 641 *C. briggsae* isotype reference strains. One isotype, XZ1213 has a high-impact *tbb-1* variant, but sampling coordinates were not recorded. The base layer of the map was obtained from the Natural Earth world countries shape file accessed via the *R* package *rnaturalearth* and function *ne_countries()*. The scale was set to return a medium-scale base map with the *scale = medium* parameter. The direct link to the base layer of the map can be accessed here: https://www.naturalearthdata.com/.
(TIF)

S23 Fig. The global distribution of *Caenorhabditis* strains that contain predicted high-impact variation in *tbb-2*. Each point represents an isotype reference strain with a predicted high-impact variant in *tbb-2*. (A) Each point corresponds to the sampling location of the strain. Each point corresponds to the location of the strain in a genome-wide phylogeny of (B) 641 *C. briggsae* and (C) 518 *C. tropicalis* isotype reference strains. The base layer of the map was obtained from the Natural Earth world countries shape file accessed via the *R* package *rnaturalearth* and function *ne_countries()*. The scale was set to return a medium-scale base map with the *scale = medium* parameter. The direct link to the base layer of the map can be accessed here: https://www.naturalearthdata.com/.
(TIF)

S24 Fig. The global distribution of *Caenorhabditis* strains that contain predicted high-impact variation in *mec-7*. Each point represents an isotype reference strain with a predicted high-impact variant in *mec-7*. (A) Each point corresponds to the sampling location of an individual *C. elegans*, *C. briggsae*, or *C. tropicalis* strain. A genome-wide phylogeny

of (B) 611 *C. elegans*, (C) 641 *C. briggsae*, and (D) 518 *C. tropicalis* isotype reference strains, where each point denotes an isotype reference strain with a predicted high-impact consequence in *mec-7*. The base layer of the map was obtained from the Natural Earth world countries shape file accessed via the *R* package *rnaturalearth* and function *ne_countries()*. The scale was set to return a medium-scale base map with the *scale = medium* parameter. The direct link to the base layer of the map can be accessed here: https://www.naturalearthdata.com/.
(TIF)

S25 Fig. The global distribution of *Caenorhabditis* strains that contain predicted high-impact variation in *tbb-4*. Each point represents an isotype reference strain with a predicted high-impact variant in *tbb-4*. **(A)** Each point corresponds to the sampling location of an individual *C. elegans*, *C. briggsae,* or *C. tropicalis* strain with a predicted high-impact consequence in the gene *tbb-4*. Each point corresponds to the location of the strain in a genome-wide phylogeny of **(B)** 611 *C. elegans*, **(C)** 641 *C. briggsae*, and **(D)** 518 *C. tropicalis* isotype reference strains. The base layer of the map was obtained from the Natural Earth world countries shape file accessed via the *R* package *rnaturalearth* and function *ne_countries()*. The scale was set to return a medium-scale base map with the *scale = medium* parameter. The direct link to the base layer of the map can be accessed here: https://www.naturalearthdata.com/
(TIF)

S26 Fig. The proportion of strains with high-impact resistant variants in beta-tubulin genes and the substrates where those strains were found. The proportion of strains (y-axis) found in a given substrate (x-axis) are displayed. Strains with a high-impact variant in a beta-tubulin gene are colored salmon. Strains with no variants in a beta-tubulin gene are colored teal. The total number of strains isolated from a given substrate is displayed above each column. Moss and rotting wood were not included in the substrate enrichment analysis due to the small sample size. No significant relationship between beta-tubulin gene variant status and substrate were identified (Fisher's Exact Test, $p = 1$).
(TIF)

S27 Fig. Multiple sequence alignment of TBB-1, TBB-2, MEC-7, TBB-4, and BEN-1 proteins from four free-living Clade V nematode species. Amino acid sequences of beta-tubulin isoforms TBB-1, TBB-2, MEC-7, TBB-4, and BEN-1 from *C. elegans* (*Cel-*), *C. briggsae (Cbr-)*, *C. tropicalis* (*Ctr-*), and *P. pacificus* (*Ppa-*) are aligned with MAFFT, and the alignment is displayed from amino acid residue 175 to residue 225. The region displayed is hypothesized to bind benzimidazoles. Residues are colored by side-chain chemical properties with the default *ggmsa* color scheme.
(TIFF)

S1 Table. *C. elegans* isotype variant table.
(TXT)

S2 Table. *C. briggsae* isotype variant table.
(TXT)

S3 Table. *C. tropicalis* isotype variant table.
(TXT)

S4 Table. *C. briggsae* and *C. tropicalis* strain pairs.
(CSV)

S5 Table. Table of CRISPR-Cas9 genome edited strains, CRISPR-Cas9 reagents, and oligonucleotide sequences.
(CSV)

S6 Table. Results from *C. briggsae* fecundity assays.
(CSV)

S7 Table. Results from *C. tropicalis* fecundity assays.
(CSV)

S8 Table. BLOSUM and Grantham scores for amino acid changes in beta-tubulin genes in the three *Caenorhabditis* species.
(TXT)

S9 Table. Conservation of embryonic expression patterns between *C. elegans* and *C. briggsae* with Jensen-Shannon gene distances estimated in *Large et al. 2024* for beta-tubulin genes Jensen-Shannon gene distances (JSD_{gene}) quantify expression conservation across homologous embryonic cell types and range from zero (conserved) to one (diverged), where values below 0.45 indicate conserved expression patterns.
(CSV)

S10 Table. Expression breadth estimates for beta-tubulin genes calculated on *C. elegans* and *C. briggsae* embryonic cells by Large *et al.* 2024 *Tau* estimates capture the cell-specific expression patterns of each gene for *C. elegans* and *C. briggsae*. Estimates range from zero (broad expression) to one (cell-type specific expression). The absolute difference between *C. elegans* and *C. briggsae Tau* is reported to reflect the divergence in cell-specificity across species for each beta-tubulin ortholog.
(CSV)

S11 Table. Neuronal cell-class expression divergence of beta-tubulin genes across *C. elegans*, *C. briggsae*, and *C. tropicalis* obtained from *Toker et al.* 2025 Jaccard distances measure the proportion of neuronal classes where gene expression differs among species. Range from zero to one, where higher values (~1) indicate that a greater proportion of cell classes express the gene in only one or two species.
(TXT)

S12 Table. Location and substrate where each isotype reference strain was collected.
(CSV)

S13 Table. Genes targeted, CRISPR-Cas9 guide RNA, and detection-primer sequences used, and mutant alleles produced in *Pristionchus pacificus.*
(TXT)

S14 Table. Beta-tubulin transcript IDs.
(TXT)

S15 Table. Manual curation of SVs.
(CSV)

S16 Table. Amino acid sequences of the BEN-1 protein for the three Caenorhabditis species.
(FA)

Acknowledgments

We would like to thank members of the Andersen laboratory for their feedback and helpful comments on this manuscript. We thank members of the *C. elegans* community for collecting the diverse set *Caenorhabditis* strains included in this study and the *Caenorhabditis* Natural Diversity Resource (NSF Capacity grant 2224885) for providing the strains for this study. We thank WormBase for providing the amino acid sequences for all six *C. elegans* beta-tubulin proteins. We thank WormBase Parasite for providing the amino acid sequences for TBB-ISOTYPE-1 beta-tubulin protein in *H. contortus*.

Author contributions

Conceptualization: Erik C. Andersen.

Data curation: Amanda O Shaver, Ryan McKeown.

Formal analysis: Amanda O Shaver, Ryan McKeown.

Funding acquisition: Erik C. Andersen.

Investigation: Amanda O Shaver, Joyce M Reyes Otero, J.B. Collins, Daniel W Hogan, James S Fraser, Stephen M Dreyer, Erik J Ragsdale.

Methodology: Amanda O Shaver, Ryan McKeown.

Project administration: Erik C. Andersen.

Resources: Erik C. Andersen.

Software: Amanda O Shaver, Ryan McKeown.

Supervision: Erik C. Andersen.

Validation: Amanda O Shaver, Ryan McKeown.

Visualization: Amanda O Shaver, Ryan McKeown.

Writing – original draft: Amanda O Shaver.

Writing – review & editing: Amanda O Shaver, Ryan McKeown, J.B. Collins, Erik C. Andersen.

References

1. Kotze AC, Gilleard JS, Doyle SR, Prichard RK. Challenges and opportunities for the adoption of molecular diagnostics for anthelmintic resistance. Int J Parasitol Drugs Drug Resist. 2020;14:264–73. https://doi.org/10.1016/j.ijpddr.2020.11.005 PMID: 33307336
2. Neff NF, Thomas JH, Grisafi P, Botstein D. Isolation of the beta-tubulin gene from yeast and demonstration of its essential function in vivo. Cell. 1983;33(1):211–9. https://doi.org/10.1016/0092-8674(83)90350-1 PMID: 6380751
3. Laclette JP, Guerra G, Zetina C. Inhibition of tubulin polymerization by mebendazole. Biochem Biophys Res Commun. 1980;92(2):417–23. https://doi.org/10.1016/0006-291x(80)90349-6 PMID: 7356473
4. Ireland CM, Gull K, Gutteridge WE, Pogson CI. The interaction of benzimidazole carbamates with mammalian microtobule protein. Biochem Pharmacol. 1979;28(17):2680–2. https://doi.org/10.1016/0006-2952(79)90049-2 PMID: 518680
5. Chalfie M, Thomson JN. Structural and functional diversity in the neuronal microtubules of Caenorhabditis elegans. J Cell Biol. 1982;93(1):15–23. https://doi.org/10.1083/jcb.93.1.15 PMID: 7068753
6. Theodorides VJ, Scott GC, Lademan MS. Strains of Haemonchus contortus resistant against benzimidazole anthelmintics. Am J Vet Res. 1970;31(5):859–63. https://doi.org/10.2460/ajvr.1970.31.05.859 PMID: 5442447
7. Roos MH, Kwa MSG, Grant WN. New genetic and practical implications of selection for anthelmintic resistance in parasitic nematodes. Parasitology Today. 1995;11(4):148–50. https://doi.org/10.1016/0169-4758(95)80136-7
8. Beech RN, Prichard RK, Scott ME. Genetic variability of the beta-tubulin genes in benzimidazole-susceptible and -resistant strains of Haemonchus contortus. Genetics. 1994;138(1):103–10. https://doi.org/10.1093/genetics/138.1.103 PMID: 8001777
9. Sangster NC, Prichard RK, Lacey E. Tubulin and benzimidazole-resistance in Trichostrongylus colubriformis (Nematoda). J Parasitol. 1985;71(5):645–51. https://doi.org/10.2307/3281438 PMID: 3840531
10. Martínez-Valladares M, Valderas-García E, Gandasegui J, Skuce P, Morrison A, Castilla Gómez de Agüero V, et al. Teladorsagia circumcincta beta tubulin: the presence of the E198L polymorphism on its own is associated with benzimidazole resistance. Parasit Vectors. 2020;13(1):453. https://doi.org/10.1186/s13071-020-04320-x PMID: 32894163
11. Venkatesan A, Jimenez Castro PD, Morosetti A, Horvath H, Chen R, Redman E, et al. Molecular evidence of widespread benzimidazole drug resistance in Ancylostoma caninum from domestic dogs throughout the USA and discovery of a novel β-tubulin benzimidazole resistance mutation. PLoS Pathog. 2023;19(3):e1011146. https://doi.org/10.1371/journal.ppat.1011146 PMID: 36862759
12. Furtado LFV, Dos Santos TR, de Oliveira VNGM, Rabelo ÉML. Genotypic profile of benzimidazole resistance associated with SNP F167Y in the beta-tubulin gene of Necator americanus helminths obtained from Brazilian populations. Infect Genet Evol. 2020;86:104594. https://doi.org/10.1016/j.meegid.2020.104594 PMID: 33080381

13. Schwenkenbecher JM, Albonico M, Bickle Q, Kaplan RM. Characterization of beta-tubulin genes in hookworms and investigation of resistance-associated mutations using real-time PCR. Mol Biochem Parasitol. 2007;156(2):167–74. https://doi.org/10.1016/j.molbiopara.2007.07.019 PMID: 17850900
14. Hahnel SR, Zdraljevic S, Rodriguez BC, Zhao Y, McGrath PT, Andersen EC. Extreme allelic heterogeneity at a Caenorhabditis elegans beta-tubulin locus explains natural resistance to benzimidazoles. PLoS Pathog. 2018;14(10):e1007226. https://doi.org/10.1371/journal.ppat.1007226 PMID: 30372484
15. Dilks CM, Hahnel SR, Sheng Q, Long L, McGrath PT, Andersen EC. Quantitative benzimidazole resistance and fitness effects of parasitic nematode beta-tubulin alleles. Int J Parasitol Drugs Drug Resist. 2020;14:28–36. https://doi.org/10.1016/j.ijpddr.2020.08.003 PMID: 32858477
16. Dilks CM, Koury EJ, Buchanan CM, Andersen EC. Newly identified parasitic nematode beta-tubulin alleles confer resistance to benzimidazoles. Int J Parasitol Drugs Drug Resist. 2021;17:168–75. https://doi.org/10.1016/j.ijpddr.2021.09.006 PMID: 34637983
17. Wit J, Dilks CM, Andersen EC. Complementary Approaches with Free-living and Parasitic Nematodes to Understanding Anthelmintic Resistance. Trends Parasitol. 2021;37(3):240–50. https://doi.org/10.1016/j.pt.2020.11.008 PMID: 33317926
18. Saunders GI, Wasmuth JD, Beech R, Laing R, Hunt M, Naghra H, et al. Characterization and comparative analysis of the complete Haemonchus contortus β-tubulin gene family and implications for benzimidazole resistance in strongylid nematodes. Int J Parasitol. 2013;43(6):465–75. https://doi.org/10.1016/j.ijpara.2012.12.011 PMID: 23416426
19. Silvestre A, Cabaret J. Mutation in position 167 of isotype 1 beta-tubulin gene of Trichostrongylid nematodes: role in benzimidazole resistance?. Mol Biochem Parasitol. 2002;120(2):297–300. https://doi.org/10.1016/s0166-6851(01)00455-8 PMID: 11897135
20. Ghisi M, Kaminsky R, Mäser P. Phenotyping and genotyping of Haemonchus contortus isolates reveals a new putative candidate mutation for benzimidazole resistance in nematodes. Vet Parasitol. 2007;144(3–4):313–20. https://doi.org/10.1016/j.vetpar.2006.10.003 PMID: 17101226
21. de Lourdes Mottier M, Prichard RK. Genetic analysis of a relationship between macrocyclic lactone and benzimidazole anthelmintic selection on Haemonchus contortus. Pharmacogenet Genomics. 2008;18(2):129–40. https://doi.org/10.1097/FPC.0b013e3282f4711d PMID: 18192899
22. Kwa MS, Veenstra JG, Roos MH. Benzimidazole resistance in Haemonchus contortus is correlated with a conserved mutation at amino acid 200 in beta-tubulin isotype 1. Mol Biochem Parasitol. 1994;63(2):299–303. https://doi.org/10.1016/0166-6851(94)90066-3 PMID: 7911975
23. Mohammedsalih KM, Krücken J, Khalafalla A, Bashar A, Juma F-R, Abakar A, et al. New codon 198 β-tubulin polymorphisms in highly benzimidazole resistant Haemonchus contortus from goats in three different states in Sudan. Parasit Vectors. 2020;13(1):114. https://doi.org/10.1186/s13071-020-3978-6 PMID: 32122383
24. Kwa MS, Kooyman FN, Boersema JH, Roos MH. Effect of selection for benzimidazole resistance in Haemonchus contortus on beta-tubulin isotype 1 and isotype 2 genes. Biochem Biophys Res Commun. 1993;191(2):413–9. https://doi.org/10.1006/bbrc.1993.1233 PMID: 8096381
25. Hurd DD. Tubulins in C. elegans. WormBook. 2018;2018:1–32. https://doi.org/10.1895/wormbook.1.182.1 PMID: 29381886
26. Wright AJ, Hunter CP. Mutations in a beta-tubulin disrupt spindle orientation and microtubule dynamics in the early Caenorhabditis elegans embryo. Mol Biol Cell. 2003;14(11):4512–25. https://doi.org/10.1091/mbc.e03-01-0017 PMID: 12937270
27. Ellis GC, Phillips JB, O'Rourke S, Lyczak R, Bowerman B. Maternally expressed and partially redundant beta-tubulins in Caenorhabditis elegans are autoregulated. J Cell Sci. 2004;117(Pt 3):457–64. https://doi.org/10.1242/jcs.00869 PMID: 14702387
28. Lu C, Srayko M, Mains PE. The Caenorhabditis elegans microtubule-severing complex MEI-1/MEI-2 katanin interacts differently with two superficially redundant beta-tubulin isotypes. Mol Biol Cell. 2004;15(1):142–50. https://doi.org/10.1091/mbc.e03-06-0418 PMID: 14565976
29. Pallotto LM, Dilks CM, Park Y-J, Smit RB, Lu BT, Gopalakrishnan C, et al. Interactions of Caenorhabditis elegans β-tubulins with the microtubule inhibitor and anthelmintic drug albendazole. Genetics. 2022;221(4):iyac093. https://doi.org/10.1093/genetics/iyac093 PMID: 35731216
30. Driscoll M, Dean E, Reilly E, Bergholz E, Chalfie M. Genetic and molecular analysis of a Caenorhabditis elegans beta-tubulin that conveys benzimidazole sensitivity. J Cell Biol. 1989;109(6 Pt 1):2993–3003. https://doi.org/10.1083/jcb.109.6.2993 PMID: 2592410
31. Gibson SB, Ness-Cohn E, Andersen EC. Benzimidazoles cause lethality by inhibiting the function of Caenorhabditis elegans neuronal beta-tubulin. Int J Parasitol Drugs Drug Resist. 2022;20:89–96. https://doi.org/10.1016/j.ijpddr.2022.10.004 PMID: 36332489
32. Collins JB, Stone SA, Koury EJ, Paredes AG, Shao F, Lovato C, et al. Quantitative tests of albendazole resistance in Caenorhabditis elegans beta-tubulin mutants. Int J Parasitol Drugs Drug Resist. 2024;25:100556. https://doi.org/10.1016/j.ijpddr.2024.100556 PMID: 38991432
33. Hahnel SR, Dilks CM, Heisler I, Andersen EC, Kulke D. Caenorhabditis elegans in anthelmintic research - Old model, new perspectives. Int J Parasitol Drugs Drug Resist. 2020;14:237–48. https://doi.org/10.1016/j.ijpddr.2020.09.005 PMID: 33249235
34. Mariene GM, Wasmuth JD. Genome assembly variation and its implications for gene discovery in nematodes. Int J Parasitol. 2025;55(5):239–52. https://doi.org/10.1016/j.ijpara.2025.01.004 PMID: 39832614
35. Crombie TA, McKeown R, Moya ND, Evans KS, Widmayer SJ, LaGrassa V, et al. CaeNDR, the Caenorhabditis Natural Diversity Resource. Nucleic Acids Res. 2024;52(D1):D850–8. https://doi.org/10.1093/nar/gkad887 PMID: 37855690
36. Shaver AO, Miller IR, Schaye ES, Moya ND, Collins JB, Wit J, et al. Quantifying the fitness effects of resistance alleles with and without anthelmintic selection pressure using Caenorhabditis elegans. PLoS Pathog. 2024;20(5):e1012245. https://doi.org/10.1371/journal.ppat.1012245 PMID: 38768235
37. Zhang G, Roberto NM, Lee D, Hahnel SR, Andersen EC. The impact of species-wide gene expression variation on Caenorhabditis elegans complex traits. Nat Commun. 2022;13(1):3462. https://doi.org/10.1038/s41467-022-31208-4 PMID: 35710766

38. Nyaanga J, Goss C, Zhang G, Ahmed HN, Andersen EJ, Miller IR, et al. Changes in body shape implicate cuticle stretch in C. elegans growth control. Cells Dev. 2022;170:203780. https://doi.org/10.1016/j.cdev.2022.203780 PMID: 35452889
39. Nyaanga J, Crombie TA, Widmayer SJ, Andersen EC. easyXpress: An R package to analyze and visualize high-throughput C. elegans microscopy data generated using CellProfiler. PLoS One. 2021;16(8):e0252000. https://doi.org/10.1371/journal.pone.0252000 PMID: 34383778
40. Henikoff S, Henikoff JG. Amino acid substitution matrices from protein blocks. Proc Natl Acad Sci U S A. 1992;89(22):10915–9. https://doi.org/10.1073/pnas.89.22.10915 PMID: 1438297
41. Grantham R. Amino acid difference formula to help explain protein evolution. Science. 1974;185(4154):862–4. https://doi.org/10.1126/science.185.4154.862 PMID: 4843792
42. Howe KL, Bolt BJ, Shafie M, Kersey P, Berriman M. WormBase ParaSite - a comprehensive resource for helminth genomics. Mol Biochem Parasitol. 2017;215:2–10.
43. Toker IA, Ripoll-Sánchez L, Geiger LT, Sussfeld A, Saini KS, Beets I, et al. Divergence in neuronal signaling pathways despite conserved neuronal identity among Caenorhabditis species. Curr Biol. 2025;35(12):2927-2945.e7. https://doi.org/10.1016/j.cub.2025.05.036 PMID: 40412379
44. Large C, Khanal R, Hillier L, Huynh C, Kubo C, Kim J. Lineage-resolved analysis of embryonic gene expression evolution in C. elegans and C. briggsae.
45. Andersen EC, Gerke JP, Shapiro JA, Crissman JR, Ghosh R, Bloom JS, et al. Chromosome-scale selective sweeps shape Caenorhabditis elegans genomic diversity. Nat Genet. 2012;44(3):285–90. https://doi.org/10.1038/ng.1050 PMID: 22286215
46. Zhang G, Mostad JD, Andersen EC. Natural variation in fecundity is correlated with species-wide levels of divergence in Caenorhabditis elegans. G3 (Bethesda). 2021;11(8):jkab168. https://doi.org/10.1093/g3journal/jkab168 PMID: 33983439
47. Schulenburg H, Félix M-A. The Natural Biotic Environment of Caenorhabditis elegans. Genetics. 2017;206(1):55–86. https://doi.org/10.1534/genetics.116.195511 PMID: 28476862
48. Crombie TA, Battlay P, Tanny RE, Evans KS, Buchanan CM, Cook DE, et al. Local adaptation and spatiotemporal patterns of genetic diversity revealed by repeated sampling of Caenorhabditis elegans across the Hawaiian Islands. Mol Ecol. 2022;31(8):2327–47. https://doi.org/10.1111/mec.16400 PMID: 35167162
49. Crombie TA, Zdraljevic S, Cook DE, Tanny RE, Brady SC, Wang Y, et al. Deep sampling of Hawaiian Caenorhabditis elegans reveals high genetic diversity and admixture with global populations. Elife. 2019;8:e50465. https://doi.org/10.7554/eLife.50465 PMID: 31793880
50. Félix M-A, Duveau F. Population dynamics and habitat sharing of natural populations of Caenorhabditis elegans and C. briggsae. BMC Biol. 2012;10:59. https://doi.org/10.1186/1741-7007-10-59 PMID: 22731941
51. Laing ST, Ivens A, Laing R, Ravikumar S, Butler V, Woods DJ, et al. Characterization of the xenobiotic response of Caenorhabditis elegans to the anthelmintic drug albendazole and the identification of novel drug glucoside metabolites. Biochem J. 2010;432(3):505–14. https://doi.org/10.1042/BJ20101346 PMID: 20929438
52. Collins JB, Dilks CM, Hahnel SR, Rodriguez B, Fox BW, Redman E, et al. Naturally occurring variation in a cytochrome P450 modifies thiabendazole responses independently of beta-tubulin. PLoS Pathog. 2025;21(1):e1012602. https://doi.org/10.1371/journal.ppat.1012602 PMID: 39808673
53. Noble LM, Yuen J, Stevens L, Moya N, Persaud R, Moscatelli M, et al. Selfing is the safest sex for Caenorhabditis tropicalis. Elife. 2021;10:e62587. https://doi.org/10.7554/eLife.62587 PMID: 33427200
54. Moya ND, Wang B, Tanny RE, Sauria MEG, O'Connor LM, Khorshidian A. Caenorhabditis briggsae ancestral genomic hyper-diversity contrasts with globally distributed genome-wide haplotypes. bioRxiv. 2025. https://doi.org/10.64898/2025.12.08.693002
55. Wang B, Moya ND, Tanny RE, Sauria MEG, O'Connor LM, Khorshidian A. Global genomic diversity of the selfing nematode Caenorhabditis tropicalis correlates with geography. bioRxiv. 2026. https://doi.org/10.64898/2026.04.05.716573
56. Athanasouli M, Witte H, Weiler C, Loschko T, Eberhardt G, Sommer RJ, et al. Comparative genomics and community curation further improve gene annotations in the nematode Pristionchus pacificus. BMC Genomics. 2020;21(1):708. https://doi.org/10.1186/s12864-020-07100-0 PMID: 33045985
57. Doyle SR, Tracey A, Laing R, Holroyd N, Bartley D, Bazant W, et al. Genomic and transcriptomic variation defines the chromosome-scale assembly of Haemonchus contortus, a model gastrointestinal worm. Commun Biol. 2020;3(1):656. https://doi.org/10.1038/s42003-020-01377-3 PMID: 33168940
58. Montarry J, Mimee B, Danchin EGJ, Koutsovoulos GD, Ste-Croix DT, Grenier E. Recent Advances in Population Genomics of Plant-Parasitic Nematodes. Phytopathology. 2021;111(1):40–8. https://doi.org/10.1094/PHYTO-09-20-0418-RVW PMID: 33151824
59. Doyle SR. Improving helminth genome resources in the post-genomic era. Trends Parasitol. 2022;38(10):831–40. https://doi.org/10.1016/j.pt.2022.06.002 PMID: 35810065
60. Stevens L, Moya ND, Tanny RE, Gibson SB, Tracey A, Na H, et al. Chromosome-Level Reference Genomes for Two Strains of Caenorhabditis briggsae: An Improved Platform for Comparative Genomics. Genome Biol Evol. 2022;14(4):evac042. https://doi.org/10.1093/gbe/evac042 PMID: 35348662
61. Moya ND, Stevens L, Miller IR, Sokol CE, Galindo JL, Bardas AD, et al. Novel and improved Caenorhabditis briggsae gene models generated by community curation. BMC Genomics. 2023;24(1):486. https://doi.org/10.1186/s12864-023-09582-0 PMID: 37626289

62. Geldhof P, Murray L, Couthier A, Gilleard JS, McLauchlan G, Knox DP, et al. Testing the efficacy of RNA interference in Haemonchus contortus. Int J Parasitol. 2006;36(7):801–10. https://doi.org/10.1016/j.ijpara.2005.12.004 PMID: 16469321

63. Roose S, Avramenko RW, Pollo SMJ, Wasmuth JD, Ame S, Ayana M, et al. Characterization of the β-tubulin gene family in Ascaris lumbricoides and Ascaris suum and its implication for the molecular detection of benzimidazole resistance. PLoS Negl Trop Dis. 2021;15(9):e0009777. https://doi.org/10.1371/journal.pntd.0009777 PMID: 34570778

64. Krücken J, Fraundorfer K, Mugisha JC, Ramünke S, Sifft KC, Geus D, et al. Reduced efficacy of albendazole against Ascaris lumbricoides in Rwandan schoolchildren. Int J Parasitol Drugs Drug Resist. 2017;7(3):262–71. https://doi.org/10.1016/j.ijpddr.2017.06.001 PMID: 28697451

65. Palma A, Matamoros G, Escobar D, Sánchez AL, Fontecha G. Absence of mutations associated with resistance to benzimidazole in the beta-tubulin gene of Ascaris suum. Rev Soc Bras Med Trop. 2020;53:e20190155. https://doi.org/10.1590/0037-8682-0155-2019 PMID: 32187331

66. Collins JB, Andersen EC. The turkey ascarid, Ascaridia dissimilis, as a model genetic system. Int J Parasitol. 2023;53(8):405–9. https://doi.org/10.1016/j.ijpara.2022.10.005 PMID: 36549442

67. Sternberg PW, Van Auken K, Wang Q, Wright A, Yook K, Zarowiecki M, et al. WormBase 2024: status and transitioning to Alliance infrastructure. Genetics. 2024;227(1):iyae050. https://doi.org/10.1093/genetics/iyae050 PMID: 38573366

68. Camacho C, Coulouris G, Avagyan V, Ma N, Papadopoulos J, Bealer K, et al. BLAST+: architecture and applications. BMC Bioinformatics. 2009;10:421. https://doi.org/10.1186/1471-2105-10-421 PMID: 20003500

69. Pertea G, Pertea M. GFF Utilities: GffRead and GffCompare. F1000Res. 2020;9:ISCB Comm J-304. https://doi.org/10.12688/f1000research.23297.2 PMID: 32489650

70. Rausch T, Zichner T, Schlattl A, Stütz AM, Benes V, Korbel JO. DELLY: structural variant discovery by integrated paired-end and split-read analysis. Bioinformatics. 2012;28(18):i333–9. https://doi.org/10.1093/bioinformatics/bts378 PMID: 22962449

71. Lesack K, Mariene GM, Andersen EC, Wasmuth JD. Different structural variant prediction tools yield considerably different results in Caenorhabditis elegans. PLoS One. 2022;17(12):e0278424. https://doi.org/10.1371/journal.pone.0278424 PMID: 36584177

72. Danecek P, Bonfield JK, Liddle J, Marshall J, Ohan V, Pollard MO, et al. Twelve years of SAMtools and BCFtools. Gigascience. 2021;10(2):giab008. https://doi.org/10.1093/gigascience/giab008 PMID: 33590861

73. Ortiz EM. Vcf2phylip v2.0: convert a VCF matrix into several matrix formats for phylogenetic analysis. Zenodo. 2019. https://doi.org/10.5281/ZENODO.2540861

74. Caro H, Dollin S, Biton A, Brancotte B, Desvillechabrol D, Dufresne Y, et al. BioConvert: a comprehensive format converter for life sciences. NAR Genom Bioinform. 2023;5(3):lqad074. https://doi.org/10.1093/nargab/lqad074 PMID: 37608802

75. Saitou N, Nei M. The neighbor-joining method: a new method for reconstructing phylogenetic trees. Mol Biol Evol. 1987;4(4):406–25. https://doi.org/10.1093/oxfordjournals.molbev.a040454 PMID: 3447015

76. Yu G. Using ggtree to Visualize Data on Tree-Like Structures. Curr Protoc Bioinformatics. 2020;69(1):e96. https://doi.org/10.1002/cpbi.96 PMID: 32162851

77. Andersen EC, Bloom JS, Gerke JP, Kruglyak L. A variant in the neuropeptide receptor npr-1 is a major determinant of Caenorhabditis elegans growth and physiology. PLoS Genet. 2014;10(2):e1004156. https://doi.org/10.1371/journal.pgen.1004156 PMID: 24586193

78. Andersen EC, Shimko TC, Crissman JR, Ghosh R, Bloom JS, Seidel HS, et al. A Powerful New Quantitative Genetics Platform, Combining Caenorhabditis elegans High-Throughput Fitness Assays with a Large Collection of Recombinant Strains. G3 (Bethesda). 2015;5(5):911–20. https://doi.org/10.1534/g3.115.017178 PMID: 25770127

79. Zamanian M, Cook DE, Zdraljevic S, Brady SC, Lee D, Lee J, et al. Discovery of genomic intervals that underlie nematode responses to benzimidazoles. PLoS Negl Trop Dis. 2018;12(3):e0006368. https://doi.org/10.1371/journal.pntd.0006368 PMID: 29601575

80. Shaver AO, Wit J, Dilks CM, Crombie TA, Li H, Aroian RV, et al. Variation in anthelmintic responses are driven by genetic differences among diverse C. elegans wild strains. PLoS Pathog. 2023;19(4):e1011285. https://doi.org/10.1371/journal.ppat.1011285 PMID: 37011090

81. Widmayer SJ, Crombie TA, Nyaanga JN, Evans KS, Andersen EC. C. elegans toxicant responses vary among genetically diverse individuals. Toxicology. 2022;479:153292. https://doi.org/10.1016/j.tox.2022.153292 PMID: 35995124

82. Shaver A, Andersen E. High-throughput larval development assay (HTLDA) v1. 2025. https://doi.org/10.17504/protocols.io.n92ldrqwng5b/v1

83. Wang C, Vidal B, Sural S, Loer C, Aguilar GR, Merritt DM, et al. A neurotransmitter atlas of C. elegans males and hermaphrodites. Elife. 2024;13:RP95402. https://doi.org/10.7554/eLife.95402 PMID: 39422452

84. Abramson J, Adler J, Dunger J, Evans R, Green T, Pritzel A, et al. Accurate structure prediction of biomolecular interactions with AlphaFold 3. Nature. 2024;630(8016):493–500. https://doi.org/10.1038/s41586-024-07487-w PMID: 38718835

85. Han Z, Lo W-S, Lightfoot JW, Witte H, Sun S, Sommer RJ. Improving Transgenesis Efficiency and CRISPR-Associated Tools Through Codon Optimization and Native Intron Addition in Pristionchus Nematodes. Genetics. 2020;216(4):947–56. https://doi.org/10.1534/genetics.120.303785 PMID: 33060138